Performance and Techno-Economic Investigation of Organic Redox Flow Batteries: An Experimental and Modeling Study

A Thesis

submitted to

Indian Institute of Science Education and Research, Pune

in partial fulfilment of the requirements for the BS-MS dual degree program

by

Rabin Siva Dev

Indian Institute of Science Education and Research, Pune

Dr. Hommi Bhabha Road, Pashan, Pune 411008, INDIA

April 2023

Supervisor: Dr.-Ing. Jens Noack

Co-supervisor: Dipl.-Ing. Daniel Gerlach

Expert member: Prof. Arun Venkatnathan

CERTIFICATE:

This is to certify that this dissertation entitled "**Performance and Techno-Economic Investigation of Organic Redox Flow Batteries: An Experimental and Modeling Study**" towards the partial fulfillment of the BS-MS dual degree program at the Indian Institute of Science Education and Research, Pune represents study/work carried out by **Rabin Siva Dev** at the Fraunhofer Institute for Chemical Technology under the supervision of Dr.-Ing. Jens Noack, Adjunct Associate Professor at UNSW, Applied Electrochemistry and Dipl.-Ing. Daniel Gerlach, Fraunhofer ICT, Applied Electrochemistry during the academic year 2022 to 2023.

Rabin Siva Dev	Dr.-Ing. Jens Noack	Dipl.-Ing. Daniel Gerlach
IISER Pune	Fraunhofer ICT	Fraunhofer ICT
20181068	Supervisor	Co-supervisor

Date: 26th March 2023

Place: Karlsruhe, Germany

DECLARATION

I hereby declare that the matter embodied in the report entitled "**Performance and Techno-Economic Investigation of Organic Redox Flow Batteries: An Experimental and Modeling Study**" are the results of the work carried out by me at the Department of Applied Electrochemistry, Fraunhofer Institute for Chemical Technology, under the supervision of Dr.-Ing. Jens Noack and Dipl.-Ing. Daniel Gerlach, and the same has not been submitted elsewhere for any other degree.

Rabin Siva Dev	Dr.-Ing. Jens Noack	Dipl.-Ing. Daniel Gerlach
IISER Pune	Fraunhofer ICT	Fraunhofer ICT
20181068	Supervisor	Co-supervisor

Date: 26th March 2023

Place: Karlsruhe, Germany

This thesis is dedicated to myself, for not giving up on the pursuit of a seemingly impossible dream over the last few years.

ACKNOWLEDGEMENTS

I express my gratitude and deep appreciation to my esteemed supervisors, Dr. Jens Noack and Mr. Daniel Gerlach, for their guidance, support, and encouragement throughout my research journey. Their invaluable insights, constructive criticism, and tireless dedication have enabled me to undertake this thesis successfully.

I would like to acknowledge Prof. Arun Venkatnathan, my expert member at IISER Pune, whose encouragement and insightful feedback greatly motivated me to put forth quality work.

I also extend my thanks to my lab mates, Akhil Challuri and Dr. Nataliya Roznyatovskaya, for sharing their innovative research ideas, discussions, and friendship during the time of research.

I would like to thank the HR and IT departments of Fraunhofer ICT, and particularly Mr. Patrik Fanz, for their irreplaceable assistance in facilitating various administrative and technical procedures, making my research journey smooth.

I extend my appreciation to Mr. Swapnil Bhuktar at IISER Pune for his invaluable assistance in procuring administrative documents and guidance for my international transfer.

I express my gratitude to KVPY, whose funding has enabled me to pursue my research and bring it to fruition.

I express my heartfelt thanks to IISER Pune for providing me with the opportunity to undertake this research and Fraunhofer ICT for providing me with the resources and infrastructure necessary for the completion of this thesis.

Finally, I would like to express my deep gratitude to my parents, family, and friends, whose unwavering support, encouragement, and love have been my source of strength and inspiration throughout my academic journey.

LIST OF FIGURES:

LIST OF TABLES:

CONTENTS:

ABSTRACT

This thesis investigates the chemical and techno-economic efficacy of Organic Redox Flow Batteries (ORFBs). Research has identified the class of redox flow batteries as a promising solution for storing renewable energy from solar and wind sources, and for grid-level applications. In particular, ORFBs stand out due to their sustainable, cost-effective, and metal-free nature.

The study focuses on two distinct ORFB systems, namely the MV/Tempol system and the AQDS/BQDS system, and compares their performance with the well-established Vanadium redox flow battery system. Different electrochemical techniques such as galvanostatic cycling, impedance spectroscopy, etc. were employed to gauge the performance parameters used in the assessment of the performance of the three battery systems.

Given the close relationship between the topic and industrial economics, a comprehensive techno-economic study was also conducted using multiple cost comparison methods, contrasting ORFBs with the already commercialized Vanadium system. For this purpose, a pre-existing techno-economic model was transformed into a desktop application, called FLOTE, which is capable of generating cost calculations and distributions. Cost analyses were then performed using the cost outputs from FLOTE.

The study emphasizes the importance of comparing large-scale energy storage systems based not only on performance but also on other equally vital parameters such as techno-economics and sustainability. FLOTE was made available as a tool for studying the techno-economics of any flow battery system. However, its full utilization also enables the generation of several battery optimization strategies, that could potentially reduce the costs of ORFBs. The experimental results revealed many primary challenges within the ORFB chemistry, to which several methods and techniques were suggested that could improve performance.

Overall, the study bridges the gap between the laboratory chemistry of ORFBs and their industrial implementation. It contributes to the development of sustainable, cost-effective, and efficient energy storage systems, which can play a critical role in enabling a more renewable and resilient energy future.

INTRODUCTION

The contemporary scientific discourse centers around the topic of sustainable and renewable energy storage technology. This trend is primarily attributed to the pressing global issues of today, such as the escalating threat of climate change due to the mounting release of greenhouse gases, energy insecurity plaguing numerous countries because of their excessive dependence on fossil fuels, and economic crisis resulting from the aftermath of the pandemic, compounded by many misguided policy choices. Consequently, the world has witnessed a significant shift in the direction of renewable energy sources such as solar and wind, reaching a share of 29% of the global electricity mix in 2020[1].

However, energy production associated with solar and wind is highly intermittent which can lead to erratic and unpredictable energy supply, resulting in energy supply-demand mismatch. To integrate solar and wind energy into the grid, an intermediatory storage system is essential to store the generated energy and provide a stable and predictable energy output to the grid at a later time.

Conventional batteries have a limited range of energy and power, and the energy-to-power ratio is restricted by their electrode and cell design. This is a limitation when it comes to directly storing from renewables, especially with scalability. Redox flow Batteries (RFBs) have garnered considerable attention in this regard as they represent a type of electrochemical energy storage where energy and power can be independently controlled.

The power output of an RFB is dependent on the battery stack size and design, while the energy output is dictated by the volume and concentration of electrolyte. Added to the independent scalability is also the ease. Energy can be scaled by increasing the quantity of active materials, whereas power can be scaled by increasing the number of cells in a stack. In conjunction with their extended cycle life, redox flow batteries are optimal for large-scale grid storage.

Currently, numerous metal-based redox flow battery (RFB) chemistries are prevalent, including all-Vanadium, Vanadium/Bromine, Iron/Chromium, and Zinc/Bromine, among others[2]. The Vanadium systems have been substantially developed and commercialized, while Zinc/Bromine and Iron/Chromium have also been partially commercialized. Nevertheless, the erratic cost of the vanadium electrolyte over the

past few years has rendered it challenging to implement at a large scale from a cost standpoint. Furthermore, non-aqueous RFBs are often considered costly and impractical for large-scale installations, particularly for grid systems[3].

This is why recent studies have focused on the development of Organic Redox Flow Batteries (ORFBs) due to their numerous advantages over other RFB systems. Organic electrolyte materials are cheaper and more abundant than their metal-based counterparts. Additionally, their mostly non-toxic and biodegradable nature adds to sustainability. Organic molecules also offer customizability, allowing for the tailored design to meet specific requirements through molecular structure modifications.

The adoption of renewable energy sources and integration of grid-scale systems, especially RFB systems, in the transition from conventional to sustainable energy sources are expected to have significant economic impacts. As large-scale industrial implementation and optimization are closely linked to the financial capacity of the executor, understanding the total and component-wise cost contributions of a battery system is equally critical in addition to understanding the chemistry. Scientific investigations of this nature, with close ties to large-scale economics, necessitate a techno-economic perspective, complementing the scientific viewpoint. To achieve a targeted and systematic reduction of system costs, the initial step involves mapping various electrochemical components and investigating their general impact on the total system cost.

As an attempt to address some of the aforementioned challenges, and with the general aim of sustainability, this study conducted experimental investigations into the performance of two ORFB systems, namely the MV/Tempol and AQDS/BQDS systems, in comparison to the well-established and optimized all-Vanadium system. In the first part, several performance parameters of each of the three battery systems were assessed using various electrochemical techniques, including galvanostatic charge-discharge cycling and electrochemical impedance spectroscopy. In the second part, a techno-economic analysis of the three battery systems was performed. To achieve this, an existing mathematical model for flow battery techno-economics, developed by Noack et al.[4], was converted into a functional desktop application, named FLOTE (FLOw battery Techno Economics) with many added functionalities. The application was utilized to generate cost data, cost distributions, and sensitivity

analysis plots. Finally, the results from the experiments and software were combined and used for overall comparisons of the three systems which include performance, techno-economics, and costs.

We believe that this study not only represents a comprehensive investigation into the chemical performance of ORFBs but also is one of the first steps taken towards transferring this technology from the laboratory to the industrial scale. FLOTE has been utilized to analyze the cost implications of implementing ORFBs, making it possible to assess the techno-economic potential of this technology prior to its entry into the market. Successful implementation of ORFBs at an industrial scale has the potential to address many of the challenges discussed so far, such as the need for cost-effective, metal-free, and sustainable energy storage solutions. Widespread adoption could also have a significant impact on reducing greenhouse gas emissions and enhancing energy security and economic stability, particularly when the world is in the face of dwindling fossil fuel reserves and soaring energy costs.

Conducted at the Fraunhofer Institute of Chemical Technology (ICT), Karlsruhe, Germany, this study was performed as part of project SONAR[5] funded by the European Union's Horizon 2020 research and innovation program. Project SONAR aims to search for truly competitive solutions for storing energy from renewable resources. The SONAR team sets out to develop a framework for the simulation-based screening of electroactive materials for ORFBs in aqueous and non-aqueous solutions with the aim of reducing the cost and time-to-market, thus strengthening the competitiveness of the EU's battery industry.

THEORY

Electrochemical Energy Storage

An electrochemical cell is a device that stores energy within its component chemicals which can later be converted into electrical energy through a redox reaction. The simplest cell consists of two electrodes; a cathode, and an anode, separated by an electrolyte solution. The electrolyte solution is such that it does not allow the passage of electrons through it but allows the passage of ions. Oxidation occurs at the anode where electrons are liberated, and reduction occurs at the cathode where electrons are consumed. If an external circuit is provided, electrons flow from the anode to the cathode, generating an electric current. This creates a charge build-up within the electrolyte which is balanced out by the movement of ions through it. The overall potential difference generated between the two electrodes determines the effective voltage of the cell and is used to power electrical devices.

Therefore, the cell potential at standard conditions, E^0_{cell}, is calculated as:

$$E^0_{Cell} = E^0_{Cathode} - E^0_{Anode} \quad (1)$$

The actual reversible cell voltage of an electrochemical cell at equilibrium depends, on the temperature T, the number of electrons n converted during the cell reaction, and the concentration of the redox species. This relationship is quantified by the Nernst equation:

$$E_{Cell} = E^0_{Cell} + \frac{RT}{nF}\, ln\left(\frac{C_{Ox}}{C_{Red}}\right) \quad (2)$$

where R describes the general gas constant, F the Faraday constant and C_{Ox} and C_{Red} the molar concentrations of the oxidizing and reducing species respectively.

There are various kinds of electrochemical energy stores such as batteries, fuel cells, capacitors, supercapacitors, etc. Out of these, batteries and fuel cells derive or store energy using chemicals, and their effective cell voltage can be determined from the Nernst Equation. The difference between batteries and fuel cells is that while batteries are used to store and convert already generated energy and have good rechargeability, fuel cells generate and provide a constant energy supply from chemical fuels, with no significance to rechargeability. Chemical energy is stored within the electrode material in batteries which is part of the cell ensemble, while in

fuel cells, chemical fuels are stored separately in fuel tanks and are pumped into the cell ensemble.

There is, however, a class of batteries that are very similar in design, engineering, and chemistry to fuel cells but share the core properties of batteries like rechargeability. These are redox flow batteries.

Redox Flow Batteries

A redox flow battery (RFB) consists of two electrolyte tanks that store two different redox-active chemicals, the positive electrolyte or the posolyte that undergoes oxidation, and the negative electrolyte or negolyte that undergoes reduction during a cell reaction. The cell stack has the cathode and anode respectively in the negolyte and posolyte compartments, and a semipermeable membrane separating the two compartments. To use the cell, the electrolytes are pumped into their respective compartments where electrochemical reactions occur on the electrode surface, charge transport occurs across the semipermeable membrane, and electrons are collected by charge collectors.

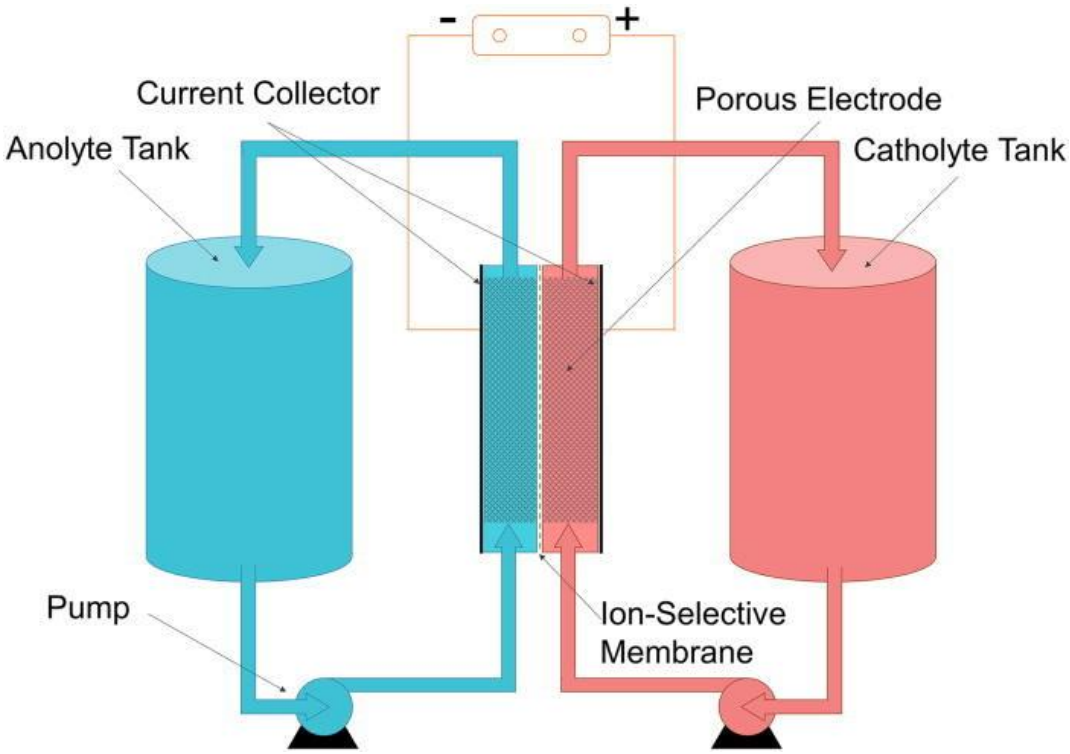

Figure 1: Schematic representation of a Redox Flow Battery Cell[6].

NASA conducted the first major experimental work on flow batteries in the 1980s, creating the iron-chromium system at the Lewis Research Center[7]. The research produced several patents, articles, and demonstrations of more than 500 cycles at 80 mA cm^{-2} current density using a bismuth-catalysed system[7]. Maria Skyllas-Kazacos created the first Vanadium flow battery at the University of New South Wales in Australia[8].

RFBs are distinguished by their ability to transform energy from flowing electrolyte media in external tanks, store it, and subsequently provide it later as needed. In effect, RFBs combine the characteristics of secondary cells such as reversibility and rechargeability, with the properties and structure of fuel cells[9]. This kind of structural design gives rise to some noteworthy features, the most important one being the almost complete separation of the scaling of energy and power[2].

The energy capacity of an RFB is primarily determined by the volume and concentration of the electrolyte used. Energy capacity increases with an increase in the volume and concentration of electrolytes. On the other hand, the power output of an RFB is determined by the electrolyte flow rate and the stack design. Increasing the flow rate and electrode surface area increases the power output of the battery. However, high flow rates can also increase the resistance of the system and lead to inefficiencies. Both energy and power also naturally depend on the electrolyte material used.

The second important feature achieved with RFB structure and chemistry is the significant ease of upscaling. In the context of systems dealing with a large amount of energy and power as in the case of storing solar and wind energy, and with large-scale implementations like integration into a grid system, upscaling is a crucial factor and most conventional batteries don’t work. Energy from the grid is also subject to a very large number of charge and discharge cycles. Hence, any energy storage system to be integrated into the grid needs a long cycle life. Like fuel cells, the two redox-active electrolytes of an RFB are stored outside in separate tanks. The separation prevents them from losing charge conferring a long cycle life to the system.

It is easy to see that the properties and design of an RFB are targeted at storing large-scale energy and an RFB setup would come out as big, stationary power plants. Consequently, such designs are unsuitable for mobile applications like vehicles and

could be impractical for small-scale storage. Other disadvantages associated with the RFB design and chemistry include the limited availability of redox-active species and poor energy densities with the existing ones.

Some additional information needing mention in order to finish the general discussion on RFBs is the semipermeable membrane and the electrodes. The membrane divides the cell into two half-spaces, one electrode per chamber on which surface the respective half-cell reactions occur. The membrane is permeable to ions of the auxiliary electrolyte or the counterions of the redox-active species but is impermeable to the redox species themselves thereby preventing them from mixing, or the so-called cross-contamination. The electrode material does not take part in the electrochemical processes as such but provides the active surface for the redox processes. It thus has a decisive influence on the performance of the battery cell and needs to have a high electrical conductivity and specific surface area while also being chemically inert to the electrolytes.

All-Vanadium Redox Flow Battery (VRFB)

The first Vanadium redox flow battery was developed and patented in the 1980s. Since then, it has been thoroughly studied and understood more than any other RFB technology from the cell to the system level. This makes it the best candidate for a reference system for ORFB studies.

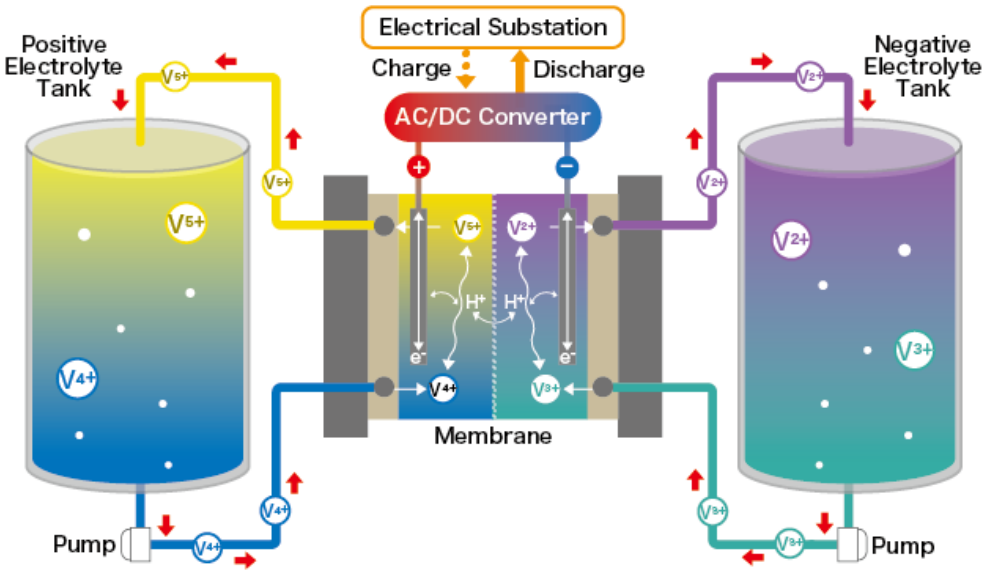

Figure 2: Structure of Vanadium Flow Battery, Copyright © LE SYSTEM CO., Ltd. All Rights Reserved.

The four oxidation states of Vanadium: V (+2), V (+3), V (+4), and V (+5), dissolved in sulphuric acid are used as redox active species.

VRFBs have the same redox-active materials in both half-cells, which is a mixture of V (+3) and V (+4). It is a symmetrical system with the advantage that diffusion-driven cross-contamination is minimized because of the same concentration of species on both sides of the half-cell and thus potentially higher energy densities are obtained. The half-cell reactions are as follows:

Posolyte reaction: $VO^{2+} + H_2O \rightleftharpoons VO_2^+ + 2\,H^+ + e^-$ $E_+^0 = 1.00\,V$

Negolyte reaction: $V^{3+} + e^- \rightleftharpoons V^{2+}$ $E_-^0 = -0.25\,V$

Cell reaction: $VO^{2+} + V^{3+} + H_2O \rightleftharpoons VO_2^+ + 2\,H^+ + V^{2+}$ $E_{Cell}^0 = 1.25\,V$

During the charging, the tetravalent VO^{2+} species in the positive half-cell are oxidized to pentavalent vanadium VO_2^+. In the negative half-cell, V^{3+} ions are reduced to V^{2+} ions. Charge balance is achieved by the migration of H^+ ions from the positive half-cell through the membrane into the negative half-cell. During discharge, all processes are reversed. A theoretical reversible cell voltage of 1.25 V is obtained.

Vanadium solutions with concentrations of 1.5 – 2.0 M are typically used in aqueous sulfuric acid, with phosphoric acid as an additive to stabilize the mixture. As electrodes, glassy carbon with graphite felts is commonly used[10], due to their stability in acidic conditions. In addition, they also show a higher overpotential for the development of hydrogen and oxygen as compared to metal electrodes. HER and OER are the most frequently occurring side reactions in aqueous-based batteries that detriment the battery capacity.

Typically used membrane separators are proton exchange membranes like Nafion, which are as little permeable as possible to Vanadium ions, or anion permeable membranes like FAP – 450 that let the sulfate anions pass through them.

Overall, VRFBs are characterized by long service lives, stability, and efficiency. VRFBs have therefore already been commercialized in upscaled form[10,11]. However, the major challenge faced by this technology is the availability of Vanadium raw

materials and the strongly fluctuating price of today's Vanadium active species[11]. The toxicity of Vanadium to both plants and animals is also a concern[2].

Methyl Viologen (MV) / 4-Hydroxy-TEMPO (Tempol) Organic Flow Batteries

The MV/4-HO-TEMPO system was first used by Liu et al.[12] and was investigated in aqueous RFBs at laboratory scales. The active materials were dissolved in Sodium chloride solution and charge equalization was made possible by the selective transport of chloride anions through an anion exchange membrane. The implemented structure is shown schematically in **Figure 3**.

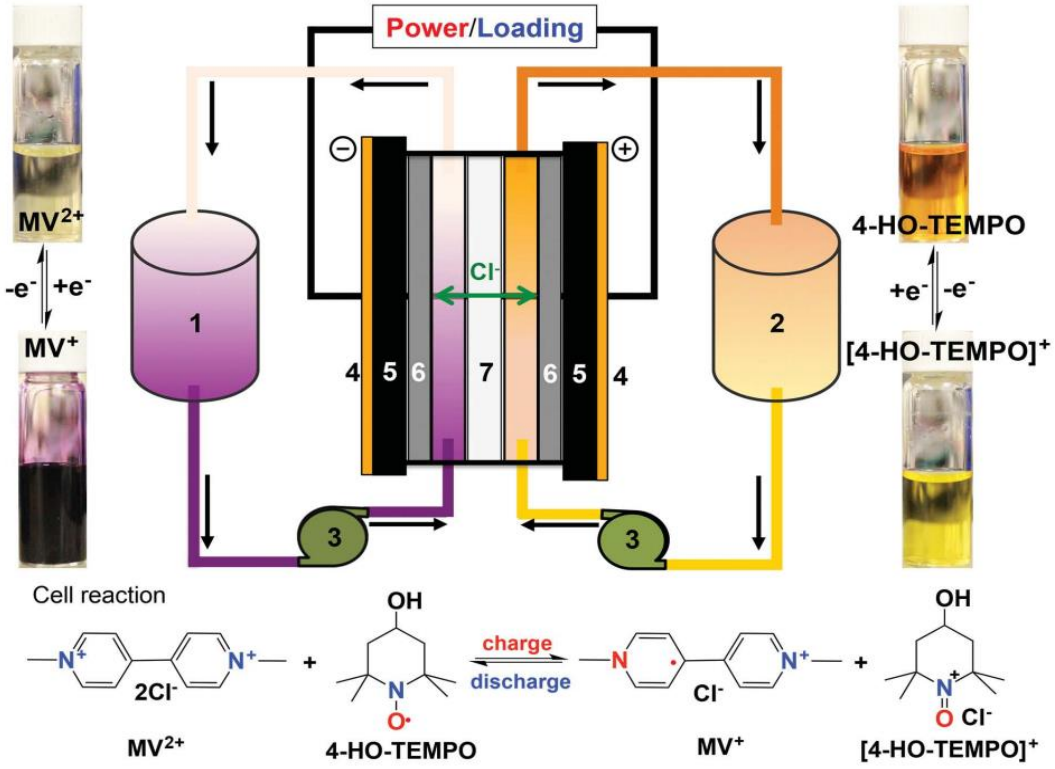

Figure 3: A schematic representation of the MV/4-HO-TEMPO organic aqueous redox flow battery (OARFB), illustrations of discharged and charged states of MV/4-HO-TEMPO, and cell reactions. Arrows indicate electrolyte flow directions. Cell components: **1)** MV anolyte reservoir **2)** 4-HO-TEMPO catholyte reservoir **3)** Pump **4)** Copper current collector **5)** Carbon end plate **6)** Graphite electrode **7)** Anion exchange membrane (AEM)[12].

The positive half-cell consists of a TEMPO derivative, 4-HO-TEMPO, which is a TEMPO molecule with an additional hydroxyl group at the 4th position. It is basically a stable heterocyclic nitroxide radical that undergoes a one-electron transfer reversible

redox reaction[9]. The negative half-cell consists of the chemical ‘paraquat’ or 1,1’-dimethyl-4,4’-bipyridinium dichloride (Methyl Viologen (MV)) which is also reversibly converted into a radical form by a one-electron transfer reaction, and the stable +2/+1 redox couple is electro-actively used[12]. The combination of both of these half-reactions gives a theoretical reversible cell voltage of 1.25 V, identical to that of Vanadium systems.

Posolyte Reaction: $E_{+}^{0} = +0.80\ V$

Negolyte Reaction: $E_{-}^{0} = -0.45\ V$

Cell Reaction: $E_{Cell}^{0} = 1.25\ V$

Figure 4: Half-cell reactions driving the MV/Tempol batteries.

It is possible to visibly follow the charging and discharging processes from the colour change of the electrolytes. In the positive half-cell, the solution of 4-HO-TEMPO in the uncharged state is coloured orange-red, while the charged solution, consisting of the $[4\text{-HO-TEMPO}]^{+}$, is yellow in colour. In the negative half-cell, the MV^{2+} solution appears pale yellow in the uncharged state. In the charged state, the MV^{+} solution shows a characteristic deep purple colour.

As in the case of most ORFBs, the MV/Tempol system too faces a challenge when it comes to long-term usability which is the occurrence of unwanted side reactions that

reduces the capacity of the system. One example is that 4-HO-TEMPO can be oxidized to a redox-inactive species by other charged $[4\text{-HO-TEMPO}]^+$ molecules[9]. Another possibility is the dimer formation of two MV^+ radicals ultimately precipitating out the poorly soluble, twice-reduced MV(0) species, which also results in the loss of redox activity[11].

Quinone-based AQDS/BQDS Organic Flow Batteries

Even though the redox properties of quinone-based organic compounds are well known, these materials have hardly been exploited for large-scale energy storage. 2,7-AQDS and BQDS are anthraquinone and benzoquinone derivatives respectively that can function together as an electrolyte couple. In 2009, Xu and Wen studied a battery system using 1,2-benzoquinone disulfonic acid as positive electrolyte solution[13]. In January 2014, Huskinson et al. reported the use of aqueous solutions of anthraquinone-2,7-disulfonic acid at the negative electrode in a redox flow battery[14].

As part of this study, we used Anthraquinone-2,7-disulfonic acid (AQDS) as the negolyte and 1,2-dihydroxybenzoquinone- 3,5-disulfonic acid (BQDS) as the posolyte. These quinones are available in their sodium salt form which is dissolved in an aqueous acid solution. Quinones undergo rapid proton-coupled electron transfer reactions without the need for dissociating high-energy bonds. With their conjugated carbon-carbon bonds and keto- and enol groups, quinones allow the delocalization and rearrangement of their pi-electrons to undergo redox transformations with extraordinary facility. Consequently, these redox couples have relatively high-rate constants for the charge-transfer process[15].

The underlying redox reactions are shown in **Figure 5**.

Posolyte Reaction:

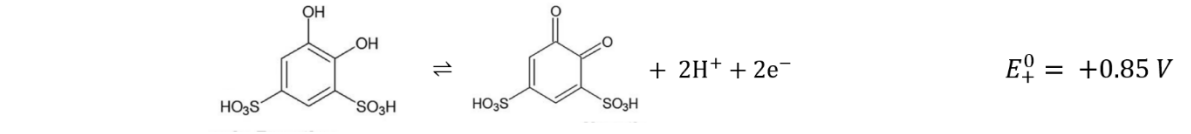

Negolyte Reaction:

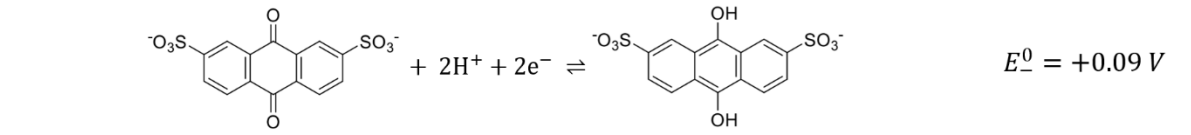

Cell Reaction:

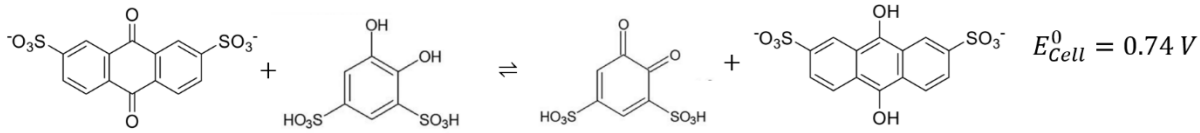

Figure 5: Redox reactions of the AQDS/BQDS system.

Quinones are used in acidic conditions in which the reduction reaction often occurs by a concerted proton and electron transfer process with the formation of no radical species. Sometimes, the mechanisms could involve sequential steps of protonation and electron transfer[15]. Alkaline environments favor the formation of radical species that tend to be reactive leading to unwanted side reactions[15]. As far as electrode materials are concerned, high-surface-area, and conductive, metal-free electrodes, such as those based on carbon black, are sufficient to support the charge-transfer process. A proton exchange membrane with a high ionic conductivity such as Nafion can be used. However, in this study, for the sake of techno-economic comparisons, the same anion exchange membrane used in the other systems, FAP – 450 was used for quinones too.

It is clear that there are several advantages presented by ORFBs like the pyridine-based MV/Tempol system or quinone-based AQDS/BQDS system. The charge-transfer overpotentials for these systems are so low that no precious metal electro-catalysts are required. Cheap carbon-based electrodes are sufficient. Organic redox couples tend to have rate constants that are 2 – 3 orders of magnitude higher than that of the Vanadium systems[15]. The standard reduction potential of an organic redox

couple is characteristic of the molecule and its specific substituent groups. Hence, one can tune the cell potential of the system by engineering the right functional groups. The substituents also heavily influence the solubility of a molecule in a given solvent. Functional groups such as the sulphonyl and hydroxy groups help in the dissolution of organic species in aqueous solvents that are polar. Organic electrolytes like quinones have also shown very good stability and tolerance at higher temperatures up to 60 degrees[15] where a conventional Vanadium system might undergo unwanted chemistries.

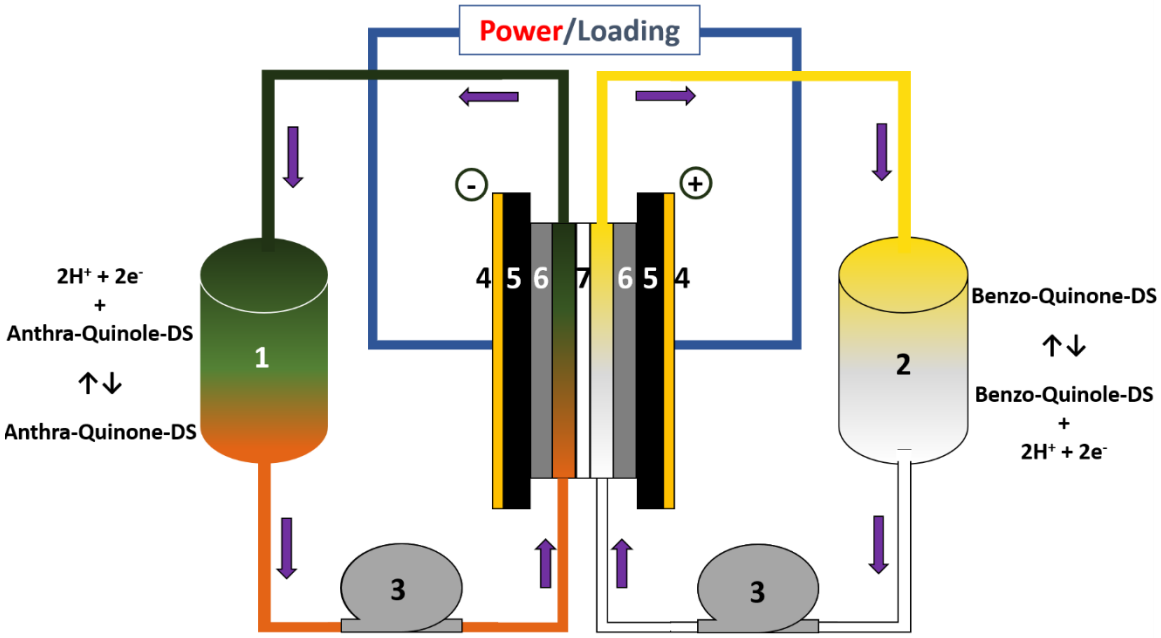

Figure 6: A schematic representation of the AQDS/BQDS organic aqueous redox flow battery. Arrows indicate electrolyte flow directions. Cell components: **1)** AQDS anolyte reservoir **2)** BQDS catholyte reservoir **3)** Pump **4)** Copper current collector **5)** Carbon end plate **6)** Graphite electrode **7)** Anion exchange membrane (FAP – 450).

Electrochemical Impedance Spectroscopy (EIS)

Electrochemical Impedance Spectroscopy (EIS) is a non-invasive test technique for measuring the impedance of a battery at various frequencies and phase shifts. The procedure entails periodically exciting the battery with a tiny voltage signal and monitoring its response. When a constant DC current is applied across a load, the resistance experienced is given by Ohm's Law. But often in real-world electrochemical scenarios, the system isn't as simple and might involve currents varying at different

rates and different directions. In such systems, there are other resistive components in addition to the ohmic resistance such as capacitive and inductive reactance. Hence, we talk about impedance which is a combination of all the different reactances. When a varying potential like a sinusoidal signal is applied across a system, the current response is not always in phase with the applied voltage. This makes impedance a complex quantity.

If an oscillating potential of $\bar{U}$ applied across a system receives a current response $\bar{I}$, then the impedance is given by the equation:

$$Z = \frac{\bar{U}}{\bar{I}} = \frac{|\bar{U}|}{|\bar{I}|} e^{i\theta} \tag{3}$$

The impedance of a system depends on the applied voltage frequency. When oscillatory perturbations with a range of frequencies are applied, one can get a spectrum of impedance. This is basically what is seen in a typical Bode plot which represents the applied frequency across the x-axis and the recorded magnitude of impedance and the phase along the y-axis.

The actual impedance of an electrochemical system is very complex but it can be estimated by oversimplifying the complex system into an equivalent Randle's circuit that represents most of the important impedance components of an electrochemical system as illustrated in **Figure 7**.

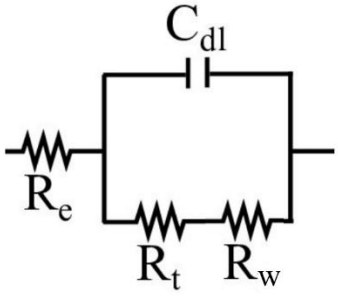

Figure 7: A simplified Randle's circuit. R_e represents the Ohmic resistance, R_t the charge-transfer resistance, R_w the Warburg resistance, and C_{dl} the double-layer capacitance.

The impedance of such a system is given as:

$$Z = R_e + \frac{R_t + R_w}{1 + i\omega(R_t + R_w)C_{dl}} \tag{4}$$

Where *I* is the imaginary number root of minus one and ω is the applied frequency. The ohmic resistance of the system is fully independent of the frequency. Hence, in the Bode plot, these are seen as typical horizontal lines parallel to the x-axis. The minimum Ohmic resistance of the system comprises of the internal resistances of all the battery components. Hence, the lowest horizontal line in a bode plot signifies the Ohmic internal resistance of a battery system. An example is given in **Figure 8**. This way it is possible to measure the ohmic resistance of an RFB by performing EIS.

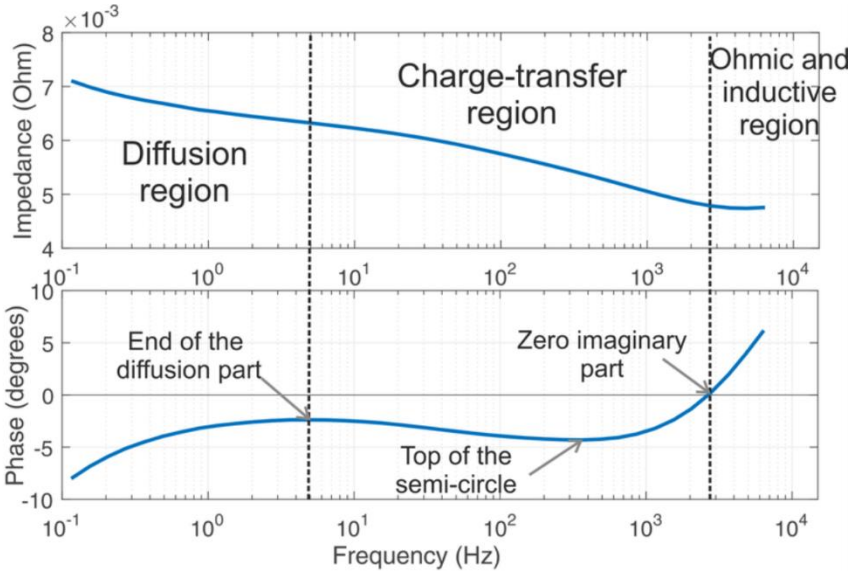

Figure 8: Bode plot of an $LiFePO_4$ cell[16].

Performance Parameters

Performance parameters are specific measured quantities used to evaluate the performance of a redox flow battery system. These are measured using various experimental techniques discussed in the methods section. The measured performance parameters are used to comprehend the level of performance of a given system and to investigate other properties such as techno-economics.

The most important performance parameters measured as part of this study are as follows:

Current density (J): It is the measure of the current *(I)* flowing per unit area of the electrode surface *(A)*. Commonly measured in units of mA cm^{-2}.

$$J = \frac{I}{A} \tag{5}$$

Theoretical volumetric capacity ($C_{Theoretical}$): Indicates the amount of charge that can be stored per volume of the RFB electrolyte. It is measured from the Concentration*I)* of the redox-active material and the number of electrons *n* transferred during the redox process and can be calculated according to Faraday's law. It is usually expressed in units of Ah L^{-1}.

$$C_{Theoretical} = nFc \tag{6}$$

where F is Faraday's constant.

Theoretical volumetric energy density ($ED_{Theoretical}$): Indicates the amount of energy that can be stored in a unit volume of the RFB electrolyte. It is calculated, by multiplying the theoretical volumetric capacity *(C)* with the theoretical reversible cell voltage *(U).* Measured in units of Wh L^{-1}.

$$ED_{Theoretical} = C_{Theoretical}U \tag{7}$$

Stored charge (Q): Determined by multiplying the charge or discharge time *(t)* with the applied current *(I).* It, therefore, corresponds to the experimentally measured capacity in units of Ah. Dividing this with the volume of electrolyte *(V)* used gives the experimental volumetric capacity of the electrolyte.

$$Q_{Charge} = It_{charge} \tag{8}$$

$$Q_{Discharge} = It_{Discharge} \tag{9}$$

$$C_{Experimental} = \frac{Q}{V} \tag{10}$$

Coulombic efficiency (CE): It is the ratio of the electrical charge introduced from the electrolyte during the charging process to that recovered in the subsequent discharging process. A 100% Coulombic Efficiency wound mean all introduced charges are recovered implying a perfectly reversible process. Deviation from 100%

Coulombic efficiency is an indicator of irreversible processes such as side reactions and cross-contaminations.

$$CE = \frac{Q_{Discharge}}{Q_{Charge}} \tag{11}$$

Voltage efficiency (VE): It is the ratio of mean discharge voltage to mean charge voltage at a constant current. The mean voltages are calculated by obtaining the area under the charge or discharge voltage curve and then dividing it by the total charge or discharge time. Voltage efficiency usually decreases with current density. This is because Voltage efficiency is an indicator of various overpotentials such as diffusion, polarization, or ohmic overpotential. And the voltage drop due to these overpotentials increases with an increase in current density in accordance with Ohm's law.

$$VE = \frac{\frac{\int_0^{t_{Discharge}} U(t)dt}{t_{Discharge}}}{\frac{\int_0^{t_{Charge}} U(t)dt}{t_{Charge}}} \tag{12}$$

Energy efficiency (EE): It is simply the product of Voltage and Coulombic efficiencies. It indicates the energy recovered during a discharge process relative to the energy supplied during the charging process.

$$EE = CE.VE \tag{13}$$

Energy density (ED): It is a measure of the energy that can be stored in a unit volume of an electrolyte. Unlike the theoretical energy density, the experimental energy density is based on the actual performance of a battery under real-world conditions. It is measured in units of Wh L^{-1}. The energy density can be calculated for both charging and discharging processes though the latter is of more scientific interest.

$$ED_{Charge} = \frac{I.\int_0^{t_{Charge}} U(t)dt}{V} \tag{14}$$

$$ED_{Discharge} = \frac{I.\int_0^{t_{Discharge}} U(t)dt}{V} \quad (15)$$

Power density (PD): This is the measure of power delivered per unit area of the electrode surface (in this context, it is not a gravimetric or volumetric quantity similar to energy density). It is measured in units of mW cm^{-2}.

$$PD_{Charge} = I\ .\ \frac{\int_0^{t_{Charge}} U(t)dt}{A.t_{Charge}} \quad (16)$$

$$PD_{Discharge} = I\ .\ \frac{\int_0^{t_{Discharge}} U(t)dt}{A.t_{Discharge}} \quad (17)$$

Techno-economic Modelling

The techno-economic model used as part of this study was created by Noack et al. in 2016[4]. The model can calculate the cost and the cost distributions of different component aspects of a redox flow battery system. According to the model, given an energy and power rating, the total cost of the flow battery system depends on the number of battery cells present in the cell stack in case of power, and the volume of electrolyte in case of energy. The model calculates the total costs from the individual costs of components.

The basic principle upon which the techno-economic model is built is the fundamental property of RFBs which is independent scaling of power and energy. The power is proportional to the number and size of the cells, whereas energy is determined by the electrolyte volume and the concentration of the active species.

$$RFB\ Costs = C_{Power} + C_{Energy} + C_{Control\ and\ Connect} \quad (18)$$

According to the model, given a power rating of P and energy rating of W, the cost of power is a function of the number of cells in the stack *(N)* and the cost of energy is a function of the volume of electrolyte used *(V)* and is calculated as shown as:

$$N = \frac{P}{I \times \overline{U_{Cell}}} \quad (19) \qquad Volume\,V = \frac{Energy\,W}{\overline{U_{Cell}} \times SoC\ range \times \frac{Fzc}{3600}} \quad (20)$$

Equations 19 and 20 shows the functional dependencies of cost of power on number of cells and the cost of energy on the volume of electrolyte used. Here, I is the applied current, U_{Cell} is the mean cell voltage, F is the Faraday constant, z is the number of electrons involved in the electrochemical reaction, and c is the concentration of the electrolyte.

The costs for power and energy can be broken down into their essential factors.

$$C_{Power} = C_{Stack} + C_{Electronics} + C_{Control\,Engineering} + C_{Fluid\,Regulation} + C_{Assembling} \quad (21)$$

The cost of control engineering depends on the cost of the sensor, actuator, and thermal regulator. Cost of Fluid regulation depends on the cost of pumps, pipes, and valves. The cost of assembling depends on the man hours and specific man-hour cost.

The expression for the cost of stack is given as:

$$\begin{aligned} &C_{Stack}(P) = \\ &C_{Assembling} + C_{Connections} + A_{Active,Cell} \cdot \left(2 \cdot C_{Endplate} + C_{Isolation\,plate} + 2 \cdot C_{Current\,collector}\right) \\ &+ \left(\frac{P}{I \cdot \overline{U_{Cell}}} \cdot A_{Active,Cell} + A_{Active,Cell}\right) \cdot C_{BPP} \\ &+2 \cdot \frac{P}{I \cdot \overline{U_{Cell}}} \cdot A_{Active,Cell} \cdot \left(C_{Felt} + C_{Frame} + C_{Gasket}\right) \\ &+ \frac{P}{I \cdot \overline{U_{Cell}}} \cdot A_{Active,Cell} \cdot C_{Membrane} \end{aligned} \quad (22)$$

where $A_{Active,Cell}$ is the active area of the cell and C_{BPP} is the cost of bipolar plate.

As shown in the previous equation, the cost of power is predominantly dependant on the cost of stack which in turn is dependent on the number of cells. The number of cells is calculated from the required power rating and the effective cell voltage.

A similar approach is adopted to calculate the cost of energy too. It mainly depends on the cost of electrolyte which in turn depends on the volume of electrolyte. The volume of electrolyte is calculated from the required energy rating and effective cell voltage.

The cost of energy is given as:

$$C_{Energy} = C_{Electrolyte} + C_{Tank} \tag{23}$$

$$C_{Electrolyte}(Energy\,W) = 2 \cdot \frac{Energy\,W}{\overline{U_{Cell}} \times SoC\ range \times \frac{F(z_1c_1 + z_2c_2)}{3600}}$$
$$\cdot (M_{Active\ Material1}c_1C_{Active\ Material\ 1} + M_{Active\ Material2}c_2C_{Active\ Material\ 2}$$
$$+ M_{Solvent}c_{Solvent}C_{Solvent} + M_{Additive\ 1}c_{Additive\ 1}C_{Additive\ 1})$$
$$+ C_{Electrolyte\ Fabrication} \tag{24}$$

where M is the molar mass of an active material, c is the molar concentration, SoC is the usable state of charge and z is the number of electrons transferred in the redox reaction.

For unsymmetrical systems like MV/Tempol or quinones, the formula for cost of electrolyte is slightly different. Instead of multiplying the cost of one electrolyte by two, the cost of the two different electrolytes is separately calculated and added together to get the final total cost. In this manner, the full cost of an RFB system is calculated in terms of a given power rating P, and energy rating W.

Further discussions on the techno-economic model would be unnecessary considering that this study focuses more on the implementation of the techno-economic model in a computer software format for fast computation and practical usability. Nevertheless, the first implementation of the model was on Microsoft Excel which was a good initial step but with limited practical usability. More about the Excel Model and the need for automation is discussed in the methods section and the application created from the Excel model is presented in the Results part.

Note: Before moving into the methods sections, one important matter needing mention is regarding the operating voltage cut-offs and stable current densities for Quinones. For Vanadium and MV/Tempol systems, these are already known but not so for quinones. So, it is part of the overall objective to first find the current densities and voltage cut-offs at which the quinone batteries are stable before their performance parameters are investigated and techno-economic analysis is performed.

METHODS AND MATERIALS

Experimental

Assembly of a standardized redox flow cell

All three battery systems investigated as part of this study were equipped with the same battery cells and components. In other words, the redox flow cells were standardized. This facilitates the direct comparisons of different systems in terms of performance and techno-economics. Many parameters in the techno-economic model become simplified with the use of standardized cells for all batteries.

Figure 9 shows the schematic representation of different parts of a standardized redox flow cell.

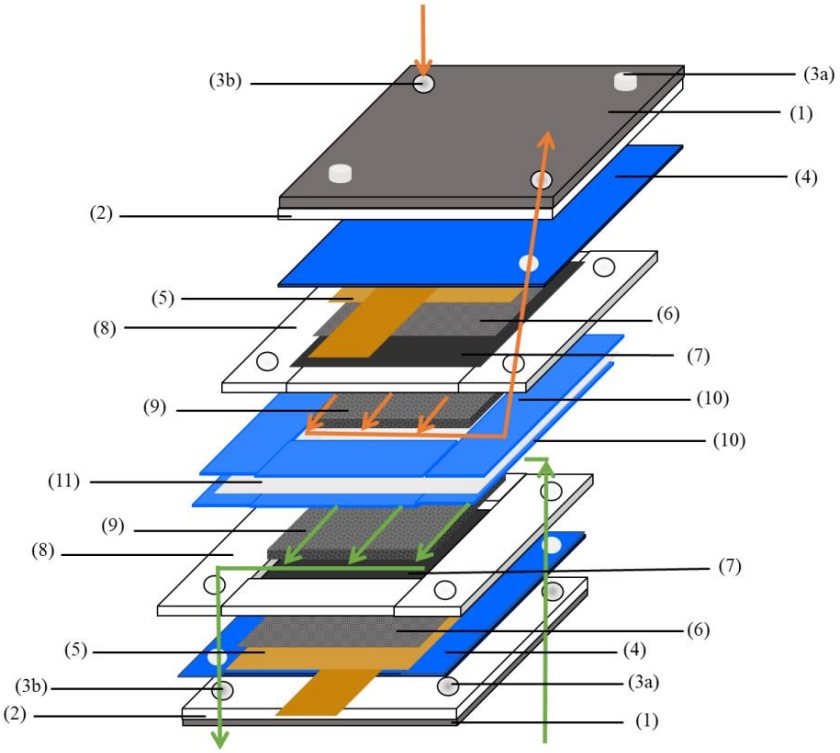

Figure 9: Schematic representation of the structure of the standardized laboratory cell with **1)** End plate, **2)** Insulation plate, **3a and 3b)** Fittings and pipe sealing caps, **4 and 10)** Seals, **5)** Current conductor, **6)** Gas diffusion layer, **7)** Bipolar plate, **8)** Flow frame, **9)** Electrode, and **11)** Membrane[17].

The functions of each part of the cell are briefly explained as follows:

1. **End plates**: The end plates hold all the components of the cell very tightly by pressing the internal components together. They are tightened with 13 screws and the tightness ensures that no electrolyte leaks out of the cell at any time. There are 4 holes on the endplate for the inlets and outlets of posolyte and negolyte materials.

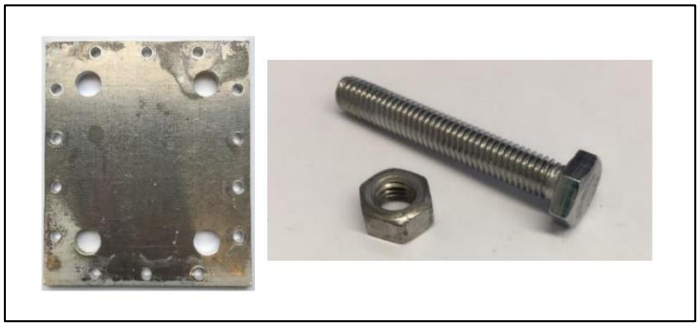

Figure 10: Aluminium endplates (**left**), screws, and bolts (**right**).

The end plates were made of Aluminium with a height of 15.5 cm, a width of 13.0 cm, and manufactured at the ICT workshop. These have 14 holes each with a diameter of 6.6 mm, into which hexagonal screws (Ø = 6 mm) with a length of 4 cm were inserted and two plates were fastened together with corresponding nuts. The four holes of inlets and outlets had a diameter of 1.6 cm.

2. **Insulation Panels**: These are insulating material lying between the end plates and the current conductors of the cell and their function is to simply make sure that the other two components are not in contact. These also have 4 holes that align with the holes of the endplates.

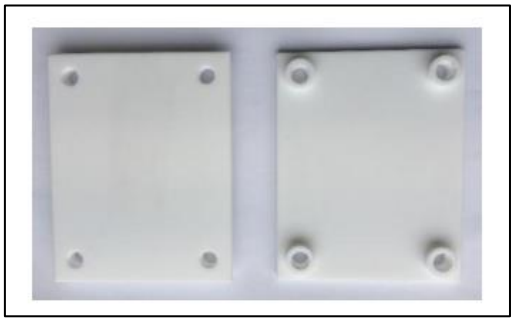

Figure 11: Teflon insulation panels.

Teflon plates were used as insulation plates. These were also manufactured at the ICT workshop and, with a height of 12.5 cm and a width of 10.0 cm, are the same size as the used flow frames. On the back, there are four holes in which an NPT1 / 8 ″ thread is integrated, into which fittings can be screwed.

3. **Fittings (3a and 3b).**: Hoses pumping the electrolyte are connected to the cell with the help of fittings. These are screwed into the endplates and insulation panels at the 4 holes. They are made of Teflon and are chemically inert to most substances.

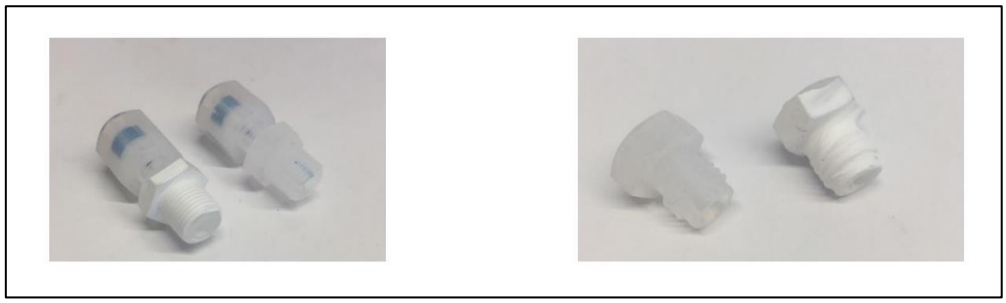

Figure 12: Fittings

For the entry and exit of the electrolyte into the cell, two straight screw connections with an NPT1 / 8 ″ external thread on one side and a D1 / 8 ″ connection on the other side from EM-Technik GmbH (exact product name: 2N100MN0318PF), were screwed into all four threads of the Teflon plate. Perfluoro alkoxy polymer compounds (PFA) were chosen for the housing material of both components due to their high chemical resistance. The threads of both components were wrapped with a layer of Teflon tape for sealing purposes.

4. **Seals**: A total of 6 seals were installed in different positions and these are meant mainly to prevent the leakage of electrolytes. One pair is put between the insulation plate and the flow frame to hold the current conductor and gas diffusion layer in place. Another pair is put between the flow frame and the membrane to seal and guide the flow of electrolytes in the right path.

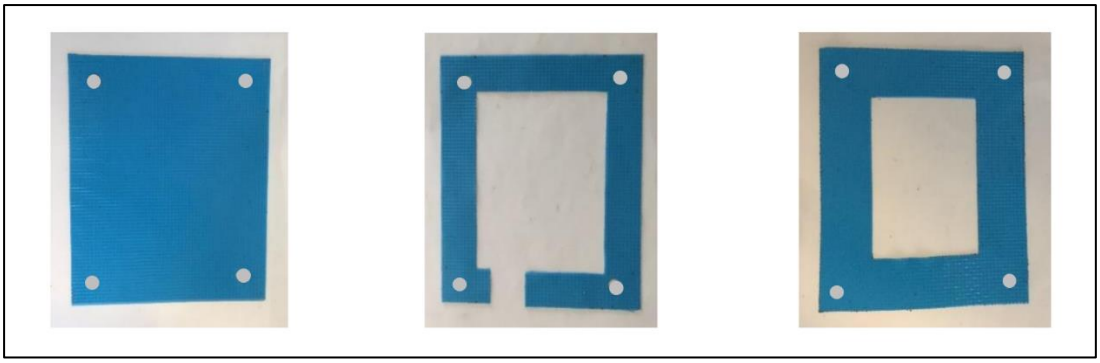

Figure 13: Seals cut into three different shapes.

Ice Cube Sealing 35 FC-PO 100 from QuinTech with a thickness of 0.5 mm was used as seals. Overall, the material was cut into three different shapes (**see Figure 13**). An area the size of a Teflon plate was cut out from the sealing material and holes are perforated where needed.

5. **Current Conductor**: This is meant to make electrical contact between the cell and any measuring device. These are usually copper plates cut to the size of the bipolar plates and are fixed on the seal right above the insulation plate.

Figure 14: Copper current collector.

Copper tape made of Cu-ETP R200 from Schlenk Metallfolien GmbH & Co. KG served as a conductor in the two half-cells. It was cut out in the size of the bipolar plate with a protruding tab that can be connected with alligator clips to the measuring instruments.

6. **Gas diffusion layer**: Due to surface imperfections between the current conducting copper plates and the bipolar plates, contact resistance arises from

the empty space between them. A gas diffusion layer eliminates such contact resistances.

The gas diffusion layer used between the copper tape and the bipolar plate was a 0.09 mm thick carbon paper from QuinTech (exact product name: GDS090S), which was cut to the same size as the carbon felt electrode.

7. **Bipolar plate**: Glassy carbon plates whose role is to transfer electrons from the felt electrode present in the reaction chamber to the current conductor through the gas diffusion layer. They also separate the felt electrode from the current conductor.

   These were made from the material SIGRADUR G from HTW Hoch Temperatur-Werkstoffe GmbH and had a height of 8.9 cm, a width of 6.4 cm, and a thickness of 3 mm. Glassy carbon material is suitable, as it is hard, has high chemical and thermal stability, and good electrical conductivity.

8. **Flow frame**: These are Teflon materials designed and produced at Fraunhofer ICT. The BPP is attached to the flow frame by Silicon glue and they also provide space for the felt electrode to occupy which basically is the reaction chamber where the half-cell reactions take place. Seals are placed on the flow frame to prevent electrolyte leakage and they are also further reinforced with adhesive tape to make fully make sure that no leakage occurs.

   Frames made from Teflon the same size as the Teflon plates were used as flow frames. On the front, they provide a reaction space with a height of 7.7 cm, a width of 5.2 cm, and a depth of 3 mm. The active usable reaction area is therefore 40 cm^2 each. Bipolar plates are fitted on the back of the frames.

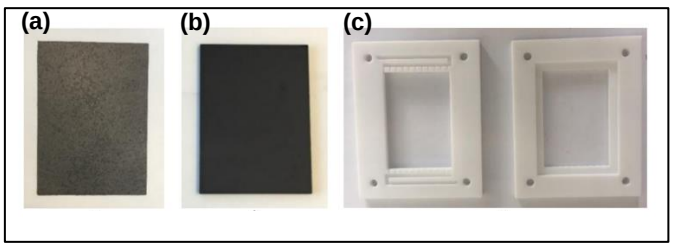

Figure 15: **a)** Gas diffusion layer **b)** Bipolar plate **c)** Flow frame.

9. **Felt Electrode**: These are absorptive materials that can drink up some electrolyte. The half-cell reactions occur within the surface of these electrodes. The nature of these materials plays a crucial role in the kinetics and chemistry of RFBs.

   The conventional 4.6 mm thick GFD 4.6 EA carbon felt from SGL Carbon was used, which had been thermally activated during the manufacturing process so that it could be cut and used directly without any further pre-treatment. It is chemically inert, and has high porosity and good electrical conductivity.
10. **Seals**: As explained in point 4.
11. **Membrane**: It separates the two half-cells from each other preventing direct contact between the redox-active species. It is also selectively permeable to certain ions thus enabling charge equalization between the two electrolytes during electrochemical reactions.

    A Fumasep FAP-450 membrane with a thickness of 50 µm from Fumatech GmbH was used. This separator is an anion exchange membrane without fabric reinforcement, which is especially suitable for VRFBs since it is stable in acidic media and has only a low permeability to vanadium ions. In addition, the membrane is characterized by a low ohmic material resistance.

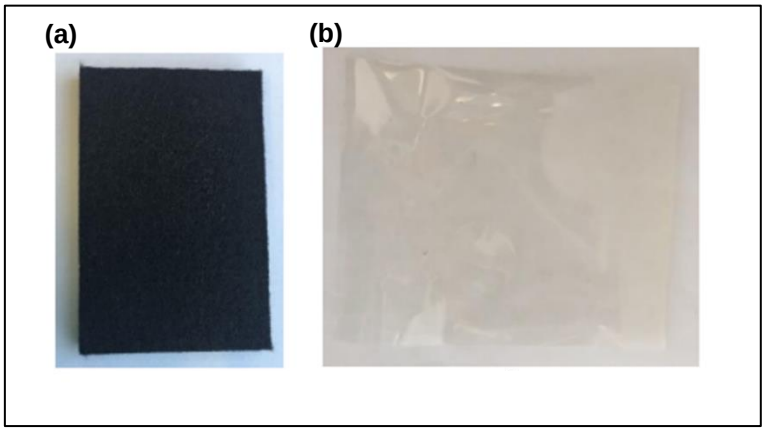

Figure 16: **a)** Carbon felt electrode, **b)** FAP-450 membrane.

Electrolytes and their preparation

Vanadium electrolyte

There was no preparation involved because Vanadium electrolyte in usable format was commercially available from GfE Metals and Materials. This consisted of a mixture of $V_2(SO_4)_3$ and $VOSO_4$ at a concentration of 1.67 M. The Vanadium compounds are dissolved in 3.8 M sulfuric acid solvent and 0.05 M phosphoric acid was present as an additive. The solution contained Vanadium in +3 and +4 oxidation states, at a ratio: V^{3+}: V^{4+} = 46.7%: 53.3%. During the first charging process, the mixture was separated into only the +3 state in the negative half-cell and only the +4 state in the positive half-cell. Both tanks were filled with 60 mL of the electrolyte, which had a dark turquoise-blue colour. This volume corresponded to a theoretical capacity of 2.67 Ah.

MV and Tempol electrolytes

45% Methyl Viologen in water was obtained from Jena Chemicals. The concentration of this solution was calculated to be 1.97 M. The molar mass of MV is 257.16 g/mol and the density of the solution was measured to be 1.1238 kg/L. 4-Hydroxy Tempol was obtained in salt form from Jena Chemicals. 1.5 M NaCl is needed in both MV and Tempol tanks to complete the preparation of the electrolytes. Experiments were planned for 0.1 M, 0.2 M, and 0.3 M electrolyte concentrations. For this 250 ml of both MV and Tempol were prepared at 0.5 M and this solution was diluted to the desired molarity during specific experiments. For the negolyte, 63.5 ml of MV solution is diluted in 186.5 ml of water. For the posolyte, 21.53 g of Tempol was first placed in a round bottom flask and water was added up to the mark.

This 0.5 M solution was used to prepare dilutions of 0.1 M and 0.3 M. To make 0.1 M, 16 ml of the electrolyte was dissolved in 64 ml of water. For 0.3 M, 48 ml of electrolyte was dissolved in 32 ml water. The total electrolyte volume was always taken to be 80 ml. 7.0128 g of NaCl was added to the 80 ml solution to obtain a 1.5 M NaCl concentration. The total volume of the solution was measured at around 85ml. The three concentrations of 0.1 M, 0.3 M, and 0.5 M provided a theoretical capacity of 0.22 Ah, 0.64 Ah, and 1.07 Ah respectively.

Quinone electrolyte

Both AQDS and BQDS are obtained in their sodium salt form from Jena Chemicals. All solutions of these compounds were prepared in 1 M H_2SO_4 which was prepared from 98% pure sulphuric acid obtained from the ICT Workshop. This sulphuric acid is 18.4 M. 20 ml of acid was dissolved in 348 ml of water to obtain 368 ml of 1 M H_2SO_4.

Similar to the previous electrolyte, 250 ml of 0.5 M each of AQDS and BQDS were prepared and they were later diluted to the desired molarity. The molar mass of AQDS and BQDS are 412.3 g/moles and 332.23 g/moles respectively. So, in 250 ml of H_2SO_4, 51.54 g of AQDS and 41.53 g of BQDS were dissolved. The salts were first put in the round bottom flask and the acid solution was filled to the mark. 0.5 M solution was then diluted to 0.1 M, 0.2 M and 0.3 M for the experiments, and their respective theoretical capacities were 0.43 Ah, 0.86 Ah, and 1.29 Ah.

Standardized Test Stand

The electrolyte flows from the electrolyte tank through the pumps into the cell and returns from the cell back into the tank through a series of hoses and connections.

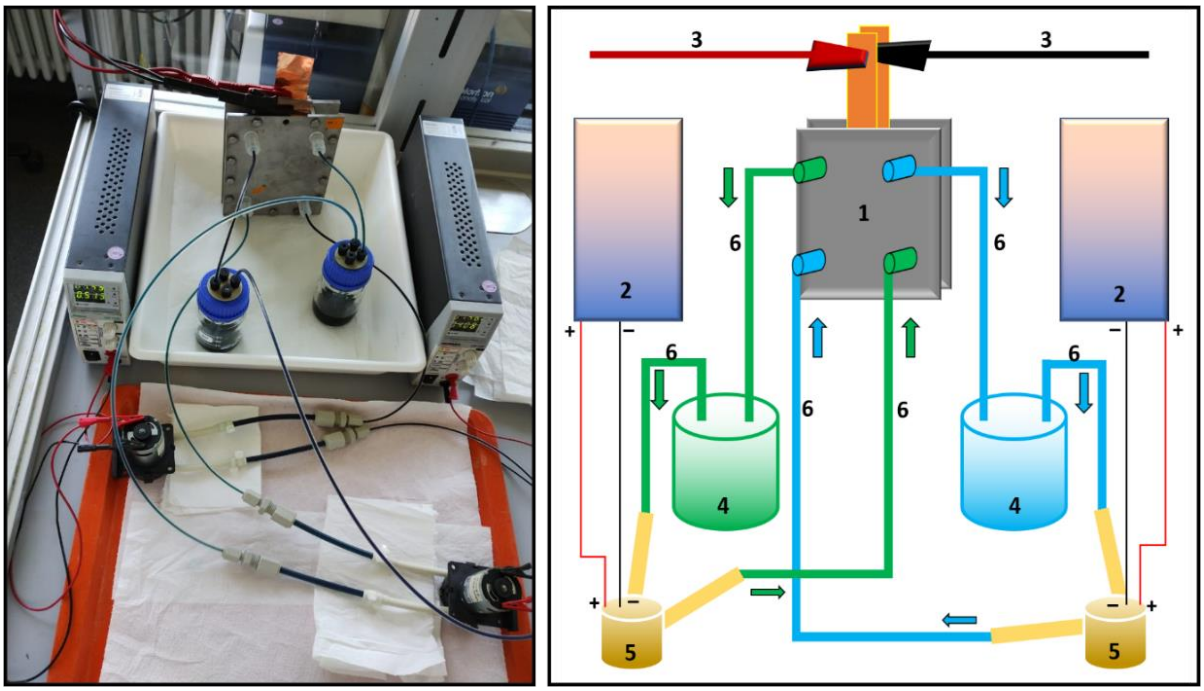

Figure 17: A standardized test stand photographed (**left**) and a schematic representation (**right**). **1)** Battery cell, **2)** Power supply for pumps, **3)** Wires connecting the cell to the instrument, **4)** Tanks, **5)** Pumps.

The standardized test stand was used for all measurements. The three main components part of the test stand are the tanks, hoses, and pumps.

Tanks: Two 100 ml screw-neck DURAN glass bottles, with a multiple distributor lid from Carl Roth were used as tanks. The lid had four openings, two of which were used for the electrolyte circuit connections and a third for a continuous in-flow of nitrogen. The last opening was left open to prevent pressure build-up.

Hoses and Circuit: PFA hoses with a diameter of 1/8 ″ from EM-Technik GmbH (exact product name: SL100S01PF10) were connected to a straight screw connection from EM-Technik (exact product name: 2N100P0503PF) which was in turn connected to a second PFA hose with a diameter of 1/4 ″ also from EM-Technik GmbH (exact product name: SL100S05PF10). These were again connected to the pump channel with the help of zip chords. The 1/8 ″ hose was connected to the lower inlets of the cell using the fittings with NPT male threads. The upper exits of the cell were connected to the electrolyte tank with another piece of the 1/8 ″ hose, thus closing the two half-cell circuits.

Pumps: Two peristaltic pumps of 12 V rating from XYZAB were used. Peristaltic pumps were cheap and it was possible to accurately control the flow rate using voltage or current. Each pump was connected to its power supply and the flow rate was calibrated with voltage before they were used in experiments.

EXPERIMENT 1: Electrochemical Impedance Spectroscopy (EIS)

Instrument: Potentiostat, Modulab XM ECS from Ametek Scientific Instruments

Analysis Software: XM-studio Software

To perform EIS using Modulab XM ECS, the XM-studio Software was opened on a PC to which the potentiostat is connected and the FRA (Frequency Response Analysis) test is selected. There were 4 cables as part of the instrument, that had to be connected to the battery cell. They were two reference electrodes of colour green and blue, the counter electrode of colour red, and a working electrode of the colour black. Red and blue were connected to the positive terminal of the cell and green and black to the negative terminal using alligator clips.

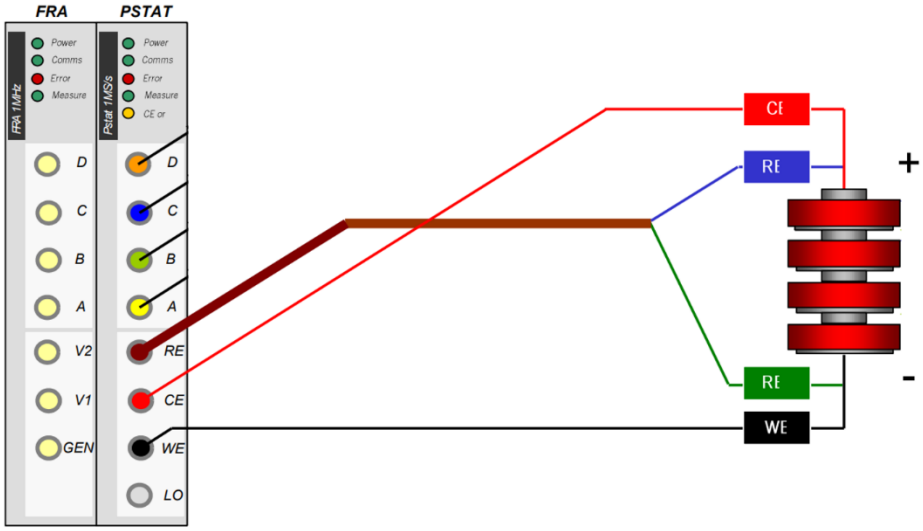

Figure 18: Representation of the connections of the Reference Electrode (RE), Working electrode (WE), and the Counter Electrode (CE) of the potentiostat to the cell terminals.

Experimental detail: The FRA test is basically a Potentiostatic EIS test. The frequency was varied from 1–100,000 Hz, with an RMS Voltage of 10 mV, and without any load. The ohmic resistance of the setup including the battery assembly and the electrolytes were obtained from a bode plot as mentioned in the theory section on EIS.

EXPERIMENT 2: Galvanostatic charge-discharge cycling

Instrument: Battery Test System, GSM series, BaSyTec GmbH

Analysis Software: BaSyTec Battery Test Software

Galvanostatic charge-discharge cycling is an experiment where a battery is charged and discharged successively between fixed voltage cut-offs at a constant current density. There are two kinds of Galvanostatic cycling performed as part of this study: A 5x5 cycling test and a degradation test.

In a 5x5 cycling test, the battery system was charged and discharged for 5 consecutive cycles at a constant current density between fixed voltage cut-offs. After each charging or discharging process, the battery was also allowed to pause for a specified time. This was repeated for 5 different current densities. 5 cycles each at 5 different current densities constituted the 5x5 cycling experiment.

In a degradation test, the battery system was charged and discharged for 50 consecutive cycles between fixed voltage cut-offs at a single current density. A pause duration after charging and discharging was present as part of this test too. The exact experimental details are shown in **Table 1**.

Battery	Experiment No. of Cycles	Voltage Cut-offs (V)	Current (A)	Pause Duration (Mins)
Vanadium	5x5 Cycling 25 Cycles	Charge = 1.65 Discharge = 0.5	1, 1.5, 2, 2.5, 3	5
	Degradation 50 Cycles	Charge = 1.65 Discharge = 0.5	2	5
MV/Tempol	5x5 Cycling 25 Cycles	Charge = 1.65 Discharge = 0.5	0.1, 0.25, 0.5, 1, 1.5	5
	Degradation 50 Cycles	Charge = 1.65 Discharge = 0.5	0.25	5
AQDS/BQDS	5x5 Cycling 25 Cycles	To be discovered as part of the study	To be discovered as part of the study	5

Table 1: Experimental details for Galvanostatic charge-discharge cycling.

The results of the above experiments were exported as text files using the Battery Test Software. This was the raw data from the experiments and all the performance parameters were calculated from this. They were then plotted using ORGINS lab plotting software.

Stepwise experimental protocol:

Step 1: Battery assembly

Step 2: Electrolyte preparation and circuit connections for test stand setup

Step 3: Inert gas bubbling (Argon/ Nitrogen) into the tanks

Step 4: Battery integration on the test setup and pump start

Step 5: OCV measurement using the Battery test system

Step 6: Electrochemical impedance spectroscopy

Step 7: Galvanostatic cycling 1 - 5x5 test

Step 8: Galvanostatic cycling 2 - Degradation test

MODELLING

For this study, the cost model converted in the form of the following hierarchical model was used. The different independent aspects of a flow battery were broken down into different levels of hierarchy and in this manner, the component-wise cost could be easily tracked and calculated.

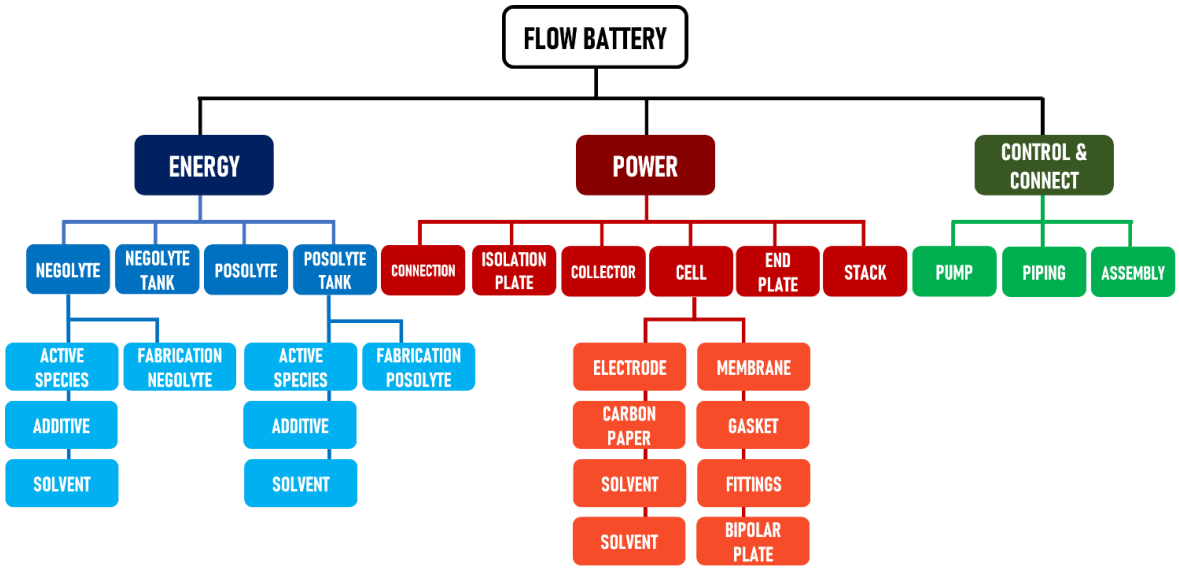

Figure 19: The hierarchical model which was directly translated into Microsoft Excel.

The above hierarchical model was already implemented on Microsoft Excel prior to this study by Noack et al[4]. Cell entries were present in an Excel sheet where all the different parameters of the battery assembly and system could be provided such as resistance values of each component, area of electrodes, concentration of electrolytes used, etc.

Features of the Excel model:

Cost outputs and distributions: The output section of the Excel model gave the different cost outputs such as the total cost of components constituting the energy and power. Both the total costs and the individual cost distributions in each sector were obtained.

Sensitivity Analysis: The dependencies from the techno-economic model implemented on MS Excel allowed one to perform Sensitivity analysis of the system in a component-by-component basis. The results were always prognostic-specific costs when varying the studied parameters in the investigated areas. When sensitivity analysis was performed practically using the Excel model, the values within the cells of the first component and the second component were varied and the changed value in the output cell was recorded each time. The process of variation was performed by manually changing the component cell entries each time. The resultant two-dimensional data was used to generate a contour plot where the first component was represented along the x-axis, the second component along the y-axis, and a heat map to represent the value of the specific cost output.

Need for the conversion of the Excel model into a software format:

It is commendable that a highly proficient techno-economic model, incorporating various cost considerations and sensitivity analyses, has been established, with Microsoft Excel serving as a noteworthy initial implementation platform. However, the Excel model does not adequately fulfill the demands for fast, effortless, and seamless execution of multiple sensitivity analyses and cost calculations. Its limitations are primarily attributed to the following deficiencies:

1. The time and effort required for the manual generation of the sensitivity analysis datasheet were painstakingly large.

2. Generation of cost distribution plots in the most comprehensible, readable, and analyzable formats was not always possible with the limited options available with MS Excel.
3. Difficulty in handling and using excessively large Excel sheets.
4. Editing the model to define a new battery system was an unsafe and difficult task due to the possibility of the original model and its dependencies getting destroyed.

All these drawbacks could be overcome by translating the Excel model into a computer software format. This would automate most of the time-consuming and laborious processes and allow room for additional functionalities such as an in-house method of plot generation. The development of a computer application was planned with the following objectives in mind:

1. Transfer the Excel-based techno-economic model into Python software with a functional UI.
2. The software needs to be standalone and must include all the parameter dependencies of the techno-economic model.
3. It needs to generate cost distribution plots of different battery systems.
4. It also needs to have the functionality to provide the cost distribution and sensitivity analyses of a custom battery system defined by user inputs.
5. It needs to automate the process of the generation of datasheets for sensitivity analysis.
6. It should perform sensitivity analysis for new parameter pairs that have not been previously explored.

For the above purpose, Python programming language was chosen to write the backend code for the app development. Python is one of the easiest to learn and most common programming languages of today[18]. This would help very well with the transfer of studies conducted so far and for future researchers to take over to resume the remaining work packages of project SONAR after this study is concluded.

For the user interface development, the desktop app development module of Python called Tkinter was used. For plotting, the Python plotting library, matplotlib was used.

Other Software tools used:

For plotting experimental data, ORIGINS Lab 2022 software was used to generate some plots. Other plots were generated by custom-written code using Python and Matplotlib.

Raw data from the Battery test system need to be processed, used in several calculations, and transformed before results consisting of the calculated performance parameters are obtained. The raw data is a text file that consists of the exact measured voltage and current values at each time step. The mean voltage during each charging and discharging cycle needs to be calculated by integrating the area under the voltage and time curve. The charge and discharge times should be calculated. The pause durations should be specifically excluded from these calculations. While it is possible to perform all of this on Origins lab software, the task is very tedious and time-consuming. Hence, to automate this process, a Python algorithm was written. The algorithm calculates the mean voltage by integrating the voltage-time curve, excluding the pause durations, and uses the results to calculate all the required performance parameters. All the performance parameters reported in the results section were calculated using this Python code. It is included in the appendix section.

RESULTS AND DISCUSSIONS

Vanadium redox flow batteries

A standardized laboratory cell was assembled, and the test stand was set up and verified to be leakproof to run the first Vanadium flow battery. N_2 gas was bubbled into the Vanadium electrolyte tank and the electrolyte was pumped into the cell. First, potentiostatic EIS was performed and the ohmic resistance of the whole system including all the cell components and electrolytes was measured. The resulting measurement was determined to be 25 mΩ which was lower than the expected range of 40-60 mΩ. At closer inspection, it was understood that the usage of the gas diffusion layer GDS090S, between the bipolar plate and the current collector, significantly reduced the contact resistance. Additionally, the bipolar plate itself made of glassy carbon also had a very low resistance. This, added with an efficient cell assembly provided a very low ohmic resistance to the standardized cell assembled for the Vanadium battery.

Galvanostatic charge-discharge experiments including the 5x5 cycling and 50 cycle degradation tests were then performed, the results of which are shown in **Figure 20**.

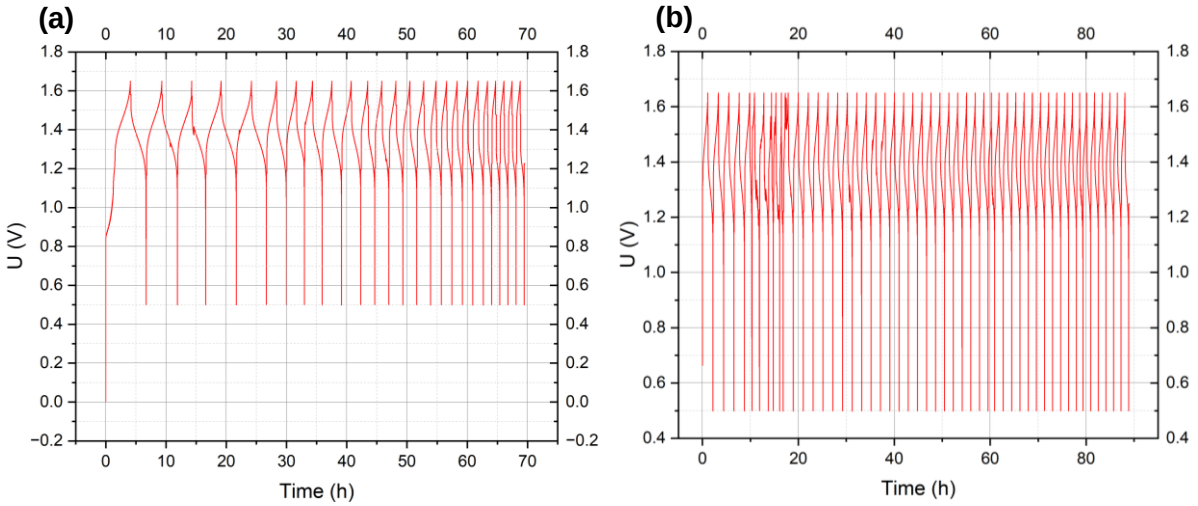

Figure 20: **a)** 5x5 cycle test results at 1-3 A, **b)** 50 cycles degradation test results at 2 A, for 1.67 M Vanadium batteries.

As seen in **Figure 20**, the periodically symmetric voltage vs time profile of the Vanadium system shows that the system is fairly stable both at the different current densities provided and for many cycles. In the degradation test, there are indeed some visible disturbances in the time frames between 10h and 20h. As evident from the rest of the plot, this disturbance fixed itself after 20h. Disturbances due to irreversible defects such as a tear in the membrane, membrane blockage after a certain level of use, or problems associated with the electrolyte must be visible in all the cycles once occurred. Since this is not the case here, it can be assumed that the above disturbance arises from a problem within the pumps, most likely an irregularity with electrolyte pumping, which fixed itself after a while. The electrolyte flow rate from the pumps is sensitive to the power supply voltage, so the disturbance could also have been due to an irregularity in the power supply.

MV/Tempol redox flow batteries

The test setup was sealed using polytetrafluoroethylene (PTFA) tape at all connection points to prevent any leakage, as one of the materials under investigation, MV, is highly toxic. The ohmic resistance of the system was measured by potentiostatic electrochemical impedance spectroscopy (EIS) and was found to exceed 10 Ω, which is an exceptionally high resistance. If an experiment similar to the galvanostatic cycling

of Vanadium is to be implemented, the minimum current required to charge or discharge the system is 1 A. However, at 1 A for MV/Tempol, the ohmic potential loss alone would be 10 Ω x 1 A, which equates to 10 V, a value significantly greater than the test termination voltage of 1.7 V. Consequently, all the supplied energy would be dissipated as ohmic loss, rendering it impossible to drive the redox reactions. Under these circumstances, cycling experiments cannot be performed as the experiment termination condition of 1.7 V is easily met during the first cycle itself, within a matter of seconds, giving rise to a voltage spike followed by experiment termination.

Figure 21a depicts the experiment termination following the voltage spike caused by high ohmic resistance. The only viable method for avoiding such voltage spikes in systems with high levels of resistance is by applying very low current densities, thus resulting in lower ohmic losses. Although performing an experiment at a very low amperage like 0.01 A lacks scientific merit, it was nevertheless carried out only to see the charging behavior of the system. So, the MV/Tempol system was subjected to a charging current of 0.01 A to maintain the ohmic loss at approximately 1 V. At this current density, the system remained free from voltage spikes and demonstrated a charging cycle, as shown in **Figure 21b**.

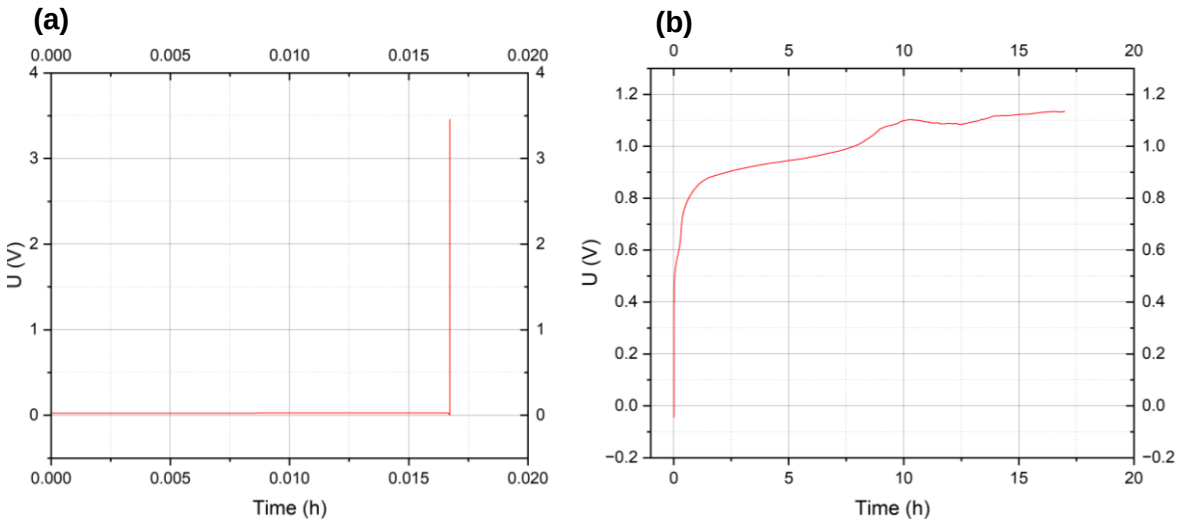

Figure 21: **a)** Voltage spike observed at 1 A, **b)** Regular charging cycle observed at 0.01 A, for 0.1 M MV/Tempol batteries.

The charging cycle at a low current of 0.01 A was observed to be remarkably long, taking more than 15 hours to complete. So, the charging process was terminated, and

the resistance of the system was measured. Very surprisingly, the measured resistance was noted to be just 50 mΩ. The system had somehow significantly reduced in resistance than the initial measurement of more than 10 Ω, following the low amperage charge cycle. To evaluate this phenomenon further, the resistance of numerous solutions of the MV/Tempol system was measured before and after the low amperage cycle. The drop in resistance was consistently observed across all measurements.

A preliminary review of the current literature on MV/Tempol revealed that this behavior had not been reported before and was, therefore, observed for the first time. It appeared that the system required some sort of 'activation cycle' of very low amperage before being able to perform electrochemically after reaching the acceptable resistance ranges. The results of multiple experiments conducted by measuring the resistance before and after the activation cycle are summarised in **Table 2**.

Concentration (M)	Ohmic resistance before Activation Cycle	Ohmic resistance after Activation Cycle
0.1	2.6 Ω	48 mΩ
0.3	15 Ω	51 mΩ
0.5	20 Ω	82 mΩ

Table 2: Resistance before and after the activation cycle.

Upon observing the reduced resistance of the system, it became feasible to conduct experiments without any premature termination, provided they were carried out within a few hours following the activation cycle. To this end, a new experimental protocol was formulated for the galvanostatic cycling of MV Tempol, outlined as follows:

Step 1: Resistance measurement by EIS

Step 2: Activation Cycle

Step 3: Post activation resistance measurement by EIS

Step 4: 5x5 cycling test

Step 5: Degradation test

Using the above protocol, galvanostatic cycling was conducted for 3 different concentrations of MV/Tempol and the results were as shown in **Figure 22**:

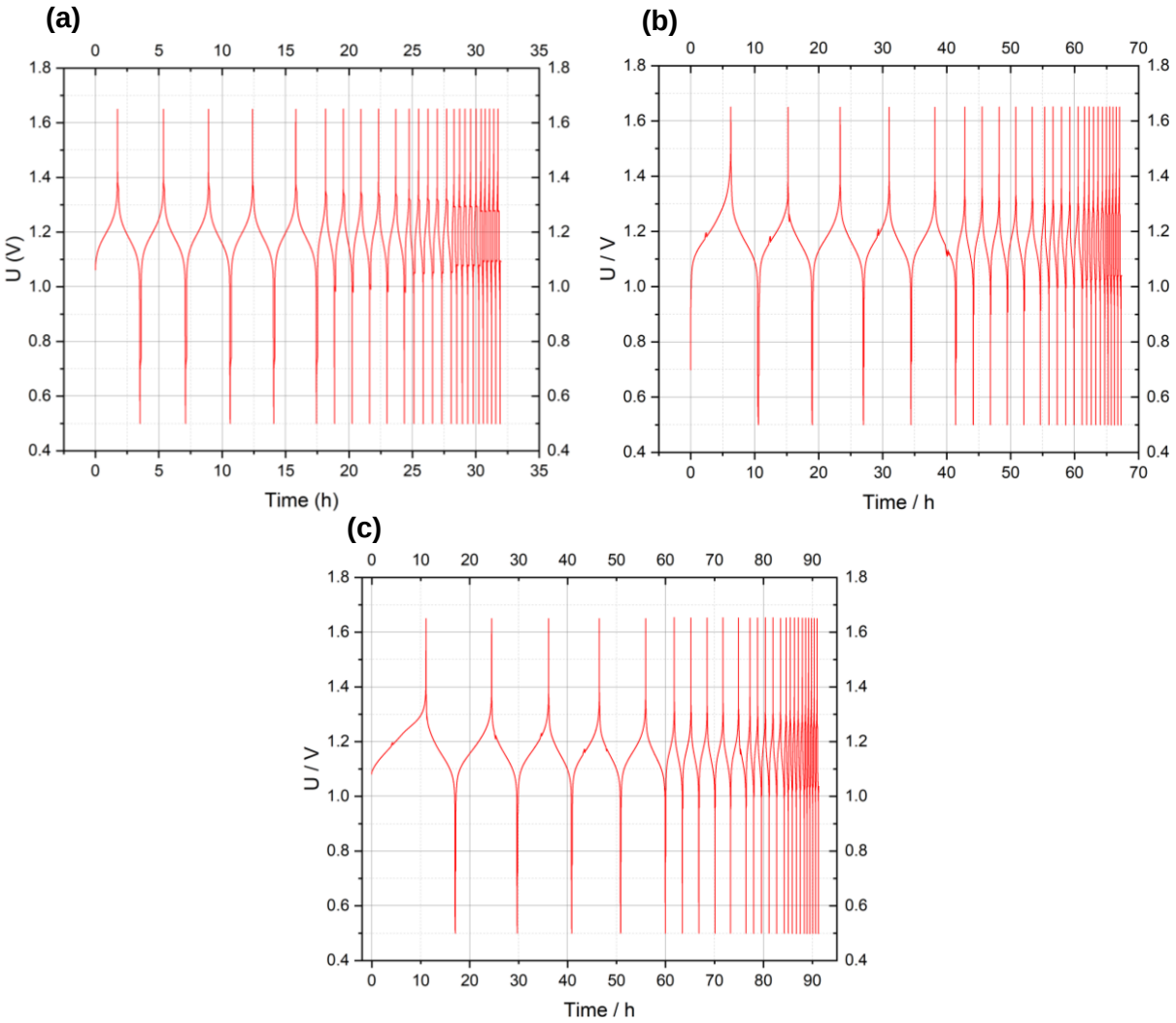

Figure 22: MV/Tempol system, **a)** 0.1 M, **b)** 0.3 M, **c)** 0.5 M, 5x5 cycling test results at currents of 0.1 A, 0.25 A, 0.5 A, 1 A, and 1.5 A.

The experimental results indicated that the cycling performance of the system exhibited good stability across all molarities. Due to the concerns regarding the initial high resistance of MV/Tempol prior to the discovery of the activation cycle, experiments were planned to operate at current levels below those employed for Vanadium systems. Specifically, cycling at 0.1 A, 0.25 A, 0.5 A, 1 A, and 1.5 A was conducted. However, higher current densities might also be achieved, because of the significant decrease in resistance following the activation cycle.

A further peculiar observation from the aforementioned plot is the very symmetrical charge-discharge profiles of MV/Tempol. This is commonly regarded as an indicator of good reversibility, reflecting a comparable rate of redox reactions during charging and discharging. Furthermore, symmetric charge-discharge cycles contribute to a high coulombic efficiency.

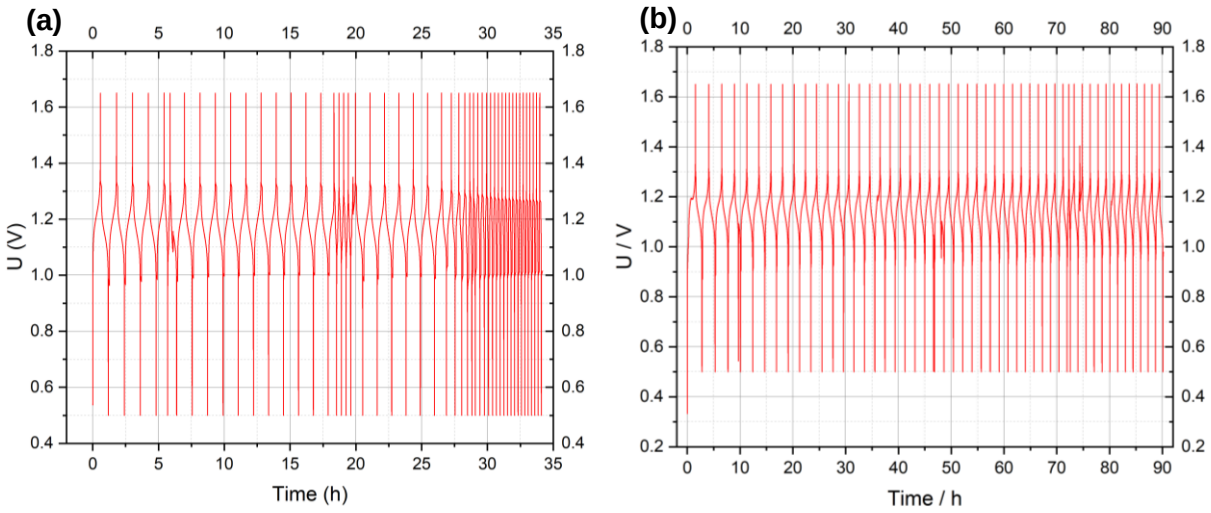

Figure 23: 50 cycles degradation test for **a)** 0.1 M MV/Tempol system, **b)** 0.5 M MV/Tempol system, at 0.25 A.

The degradation tests too demonstrated a considerable degree of stability, particularly for the 0.5 M concentration, which hardly experienced any disturbances. The disturbances observed for 0.1 M approximately at 5 and 20 h, were most likely attributed to pump issues that had been previously identified with the Vanadium case. However, the narrowing of cycles from approximately 27 h, which persisted until the end of the reaction, may suggest permanent defects, such as side reactions or cross-contamination, which were quite likely possible after prolonged usage. Upon disassembling the 0.1 M battery, some internal leakages were observed, something which was completely absent in the 0.5 M battery. So, there might be a chance that a more robust battery assembly with minimal internal leakages may enhance the stability and performance of the batteries.

AQDS/BQDS redox flow batteries

As previously mentioned, the optimal operating voltages, current densities, and electrolyte concentrations for AQDS/BQDS batteries for galvanostatic cycling were initially unknown. Consequently, the first objective of this section was to identify the optimal operating conditions before assessing and analyzing performance.

The resistance of the AQDS/BQDS system was measured to be 25 mΩ in a 2 M H_2SO_4 solvent, comparable to that of vanadium systems. Given that this is an organic system, the voltage ranges and current densities typically employed for MV/Tempol were utilized as the initial operating parameters. All the experiments performed to arrive at the optimal operating conditions are (qualitatively) listed below.

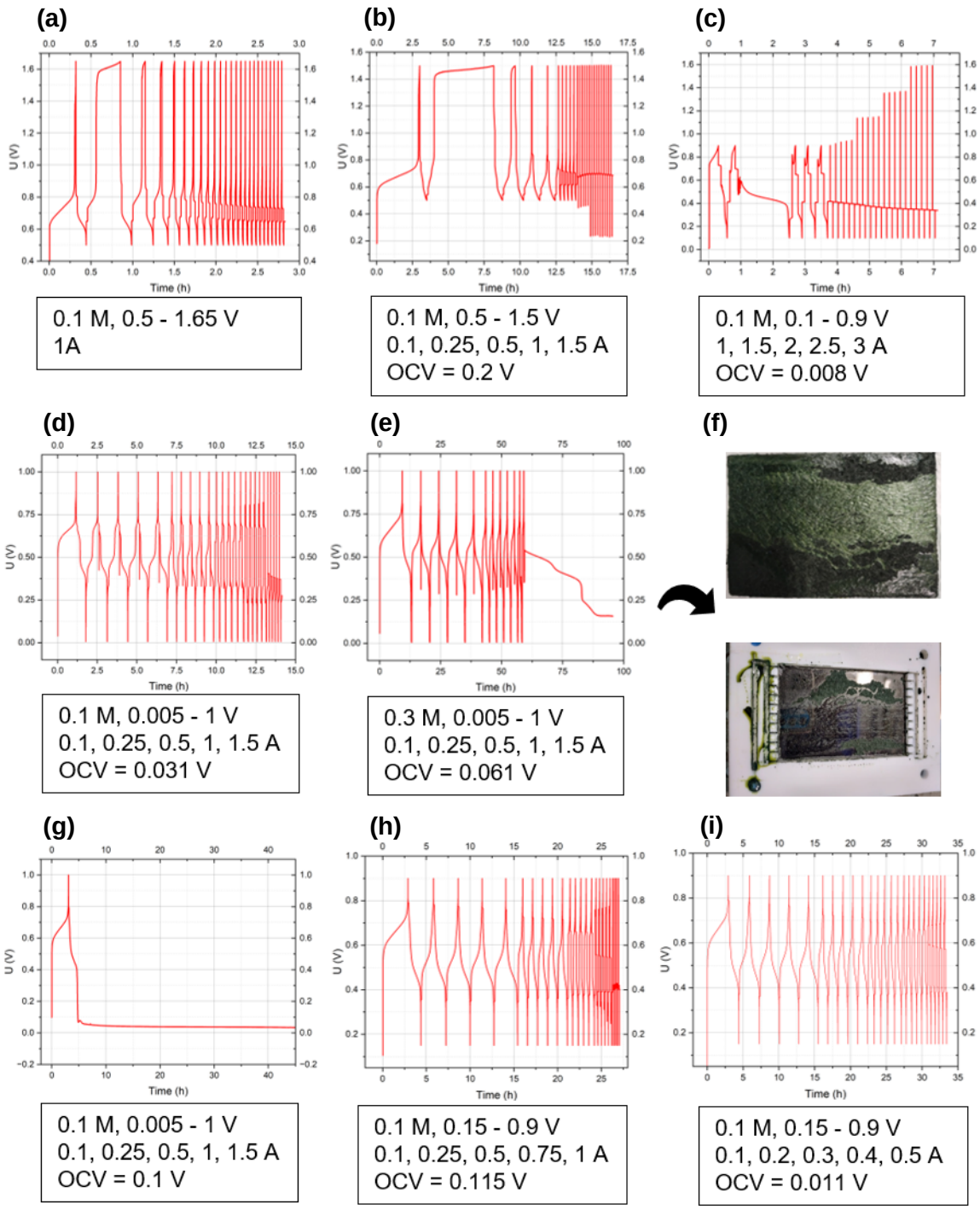

Figure 24: Screening procedure adopted to find out the optimal operating conditions.

Galvanostatic cycling of the AQDS/BQDS system was initiated at a voltage range equivalent to MV/Tempol but at a constant current of 1 A, in 2 M sulphuric acid solvent, yielding the curve depicted in **Figure 24a**. However, a stable set of cycles was not obtained, and one particular slow side reaction was notably apparent following the first discharge, visible in the second charging cycle. The solubility of quinones in 1 M sulphuric acid is greater than in 2 M[19]. Accordingly, the experiment was repeated, but the current was changed to the range utilized for MV/Tempol and using 1 M sulphuric acid. The results are presented in **Figure 24b**, which resembled those of the initial experiment. Consequently, it was inferred that the issue stemmed from the voltage range utilized.

Baur et al. used the voltage range of 0.005 V – 1 V for their AQDS/BQDS batteries[19]. So, cycling was performed in this voltage range first at low currents of 0.1 A, 0.25 A, 0.5 A, 1 A, 1.5 A as shown in **Figure 24d**, and then at high currents of 1 A, 1.5 A, 2 A, 2.5 A, 3 A as shown in **Figure 24c**. The system was clearly very unstable at higher current densities with large ohmic losses. So, all further experiments were conducted at low current densities.

Even in the new voltage and low current densities ranges, the system wasn't fully stable as seen from the odd spikes in each discharge cycle (**Figure 24d**). When those same ranges were provided to 0.3 M electrolyte, the system failed to discharge after a certain limit due to the formation of an insoluble solid precipitate on the surface of the carbon electrodes and the bipolar plate as shown in **Figure 24f**. Due to such instability at higher concentrations, all further experiments were conducted at concentrations lower than 0.3 M.

Another experiment performed with 0.1 M electrolyte (**Figure 24g**) showed that the spikes in the discharge cycle could be because of the very low voltage of 0.005 V up to which the system was being discharged, which was much lesser than the system open circuit voltage. In **Figure 24g**, it was apparent that when the system OCV was 0.1 V, it struggled to discharge to 0.005 V which was far away from the OCV. So, the discharge voltage cut-off was raised to 0.15 V so that it was not too far away from the OCV. This indeed removed all the disturbances in the discharge cycle as shown in **Figure 24h**. The uneven spikes during discharge did not appear anymore.

Figure 24h also shows that the system is fairly stable at 0.1 A, 0.25 A, and 0.5 A but not as much at 0.75 A and 1 A. So, the current range was chosen to be from 0.1 A to 0.5 A. Thus, from the above set of eight experiments, the stable operating voltage range was found to be 0.15 V - 0.9 V, and currents up to 0.5 A could be provided. A maximum of 0.3 M electrolyte concentration gave stable outputs.

New galvanostatic cycling was performed at the stable voltage and current ranges with 0.1 M, 0.2 M, and 0.3 M electrolyte concentrations, the results of which were as shown in **Figure 25**.

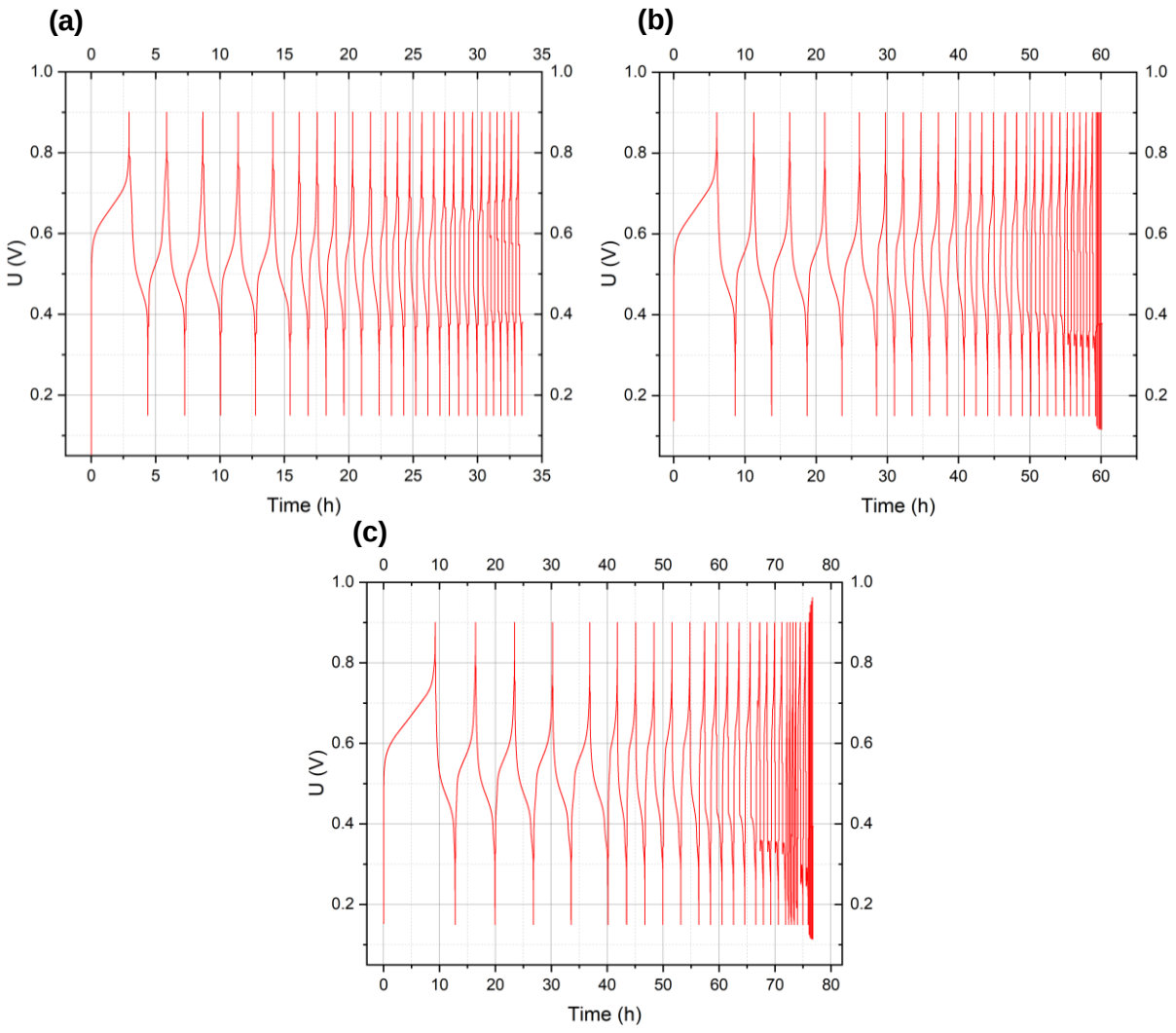

Figure 25: AQDS/BQDS system, **a)** 0.1 M, **b)** 0.3 M, **c)** 0.5 M, 5x5 cycling test results at currents of 0.1, 0.2, 0.3, 0.4, and 0.5 A.

The ohmic resistance of 0.1 M, 0.2 M, and 0.3 M ADQDS/BQDS systems were measured to be 70 mΩ, 92 mΩ, and 80 mΩ respectively.

It was also interesting to see that the OCV of systems was highly variable. One reason for this could be that the OCV of a freshly prepared uncharged electrolyte system that was untested was affected by the small amounts of droplets of charged electrolytes from previous experiments remaining within the pump tubes or the connecting hoses. When new electrolytes were run through the same pumps and hoses through which the previous electrolyte had passed through, they get mixed with a small amount of residual and unremoved charged electrolytes from past experiments. This could affect both the system OCV as well as the system resistance although this does not really affect the galvanostatic cycling experiments.

From **Figure 25**, it is evident that the first charging cycle of the system is longer than all subsequent cycles. This phenomenon may be attributed to the use of some of the energy from charging for the initial development of a stable passivating film on the electrode surface with a slow rate of formation, during the first cycle. Once this stable layer was established, most of the energy was consumed for redox reactions which occurred at higher rates.

Performance instability at higher current densities was visible in the final hours of cycling in **Figure 25b and 25c** for higher concentrations. This decline in performance at higher concentrations could indicate an issue with the electrolyte, and as shown in **Figure 25**, the instability was primarily due to higher ohmic losses at high currents. This might suggest that the electrolyte's resistance was dependent on the current and increased with an increase in current. However, a more comprehensive understanding is feasible only by analyzing the performance parameters.

PERFORMANCE PARAMETERS

All the performance parameters described in the theory section could be calculated from galvanostatic cycling experiments. These were calculated for all three battery systems (V, MVT, and Quinones) and were compared in the following section.

Comparison of Coulombic Efficiency

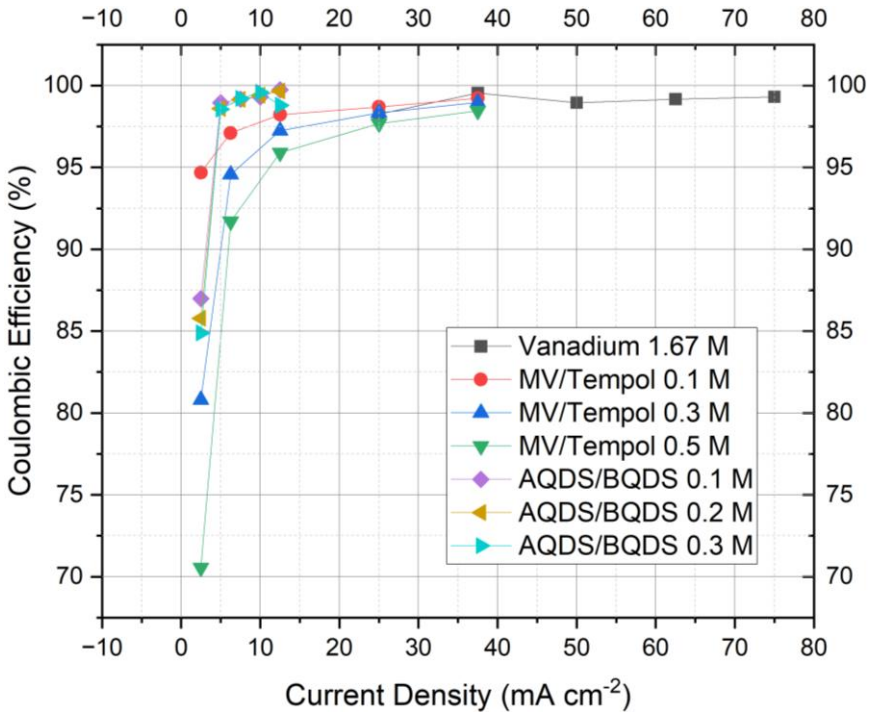

Figure 26: Comparison of Coulombic Efficiencies.

By comparing the Coulombic Efficiency (CE) of different systems, what is in effect being compared is the efficiency of conversion of the provided electrical energy during the charging cycle into reversible chemical energy stored as charge in the system. It was seen that the CE of organic systems was very less at the smallest current density. This could be attributed to the energy lost during the first charging cycle for the formation of a stable layer across the electrode surface as discussed earlier. CE of the MV/Tempol system is less than both quinones and Vanadium and decreased with an increase in concentration. One possibility for this was the occurrence of side reactions. Some part of the energy provided was used up for irreversible side reactions, the rate of which would be higher at higher initial concentrations hence the decrease at higher concentrations. Studies have shown that the posolyte pH decreased from neutral to weakly acidic during cycling, and the reversibility of Tempol deteriorated because of its side reactions in acid[20]. In fact, this was even visible as a solid deposit at the bottom of Tempol electrolyte tanks after cycling, most conspicuously for 0.5 M.

Quite contrary to what was expected for organics, quinones showed excellent CE almost reaching 100 percent efficiency at 0.5 A current density. This was even greater than that of Vanadium systems. This was an indicator that the redox reactions involved

in the quinone-hydroquinone interconversion had excellent reversibility and kinetics without many side reactions as seen in typical electrochemical systems with good CE. Unlike MV/Tempol, quinones consistently showed the same CE even at higher concentrations reinforcing the conclusion of minimal side reactions.

Comparison of Voltage Efficiency

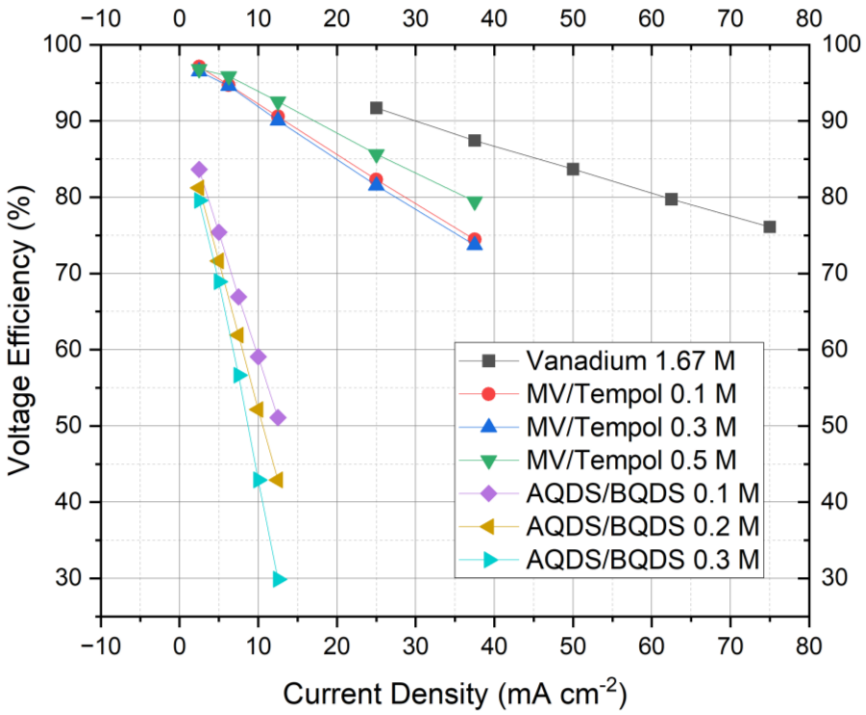

Figure 27: Comparisons of Voltage Efficiencies.

Comparison of Voltage Efficiency (VE) as shown in the previous plot presents a comparison of the effectiveness of charge and electron transport within the system. VE was found to linearly decrease with current density for all systems. This is due to the increased IR drop and concentration polarisations at higher current densities reflected predominantly in the discharging cycles.

The voltage efficiency (VE) of organic systems (especially quinones) was considerably lower than that of the Vanadium system. This difference did not arise from the initial ohmic resistances of the systems since they were roughly 25 mΩ, 60 mΩ, and 70 mΩ for Vanadium, MV/Tempol, and quinones respectively, which weren't too far apart. So, it was assumed that there was some sort of development of charge transport

resistance during successive cycles. In the case of quinones, using an additive like NaCl as in the MV/Tempol case to reduce the charge transport resistance could be tried out. Additionally, it can also be observed that the VE of Quinones decreased with an increase in concentration, which was an indicator of a problem within the electrolyte. Such a concentration dependant trend could also be due to the usage of an anion-permeable membrane. The only transferable anions available in the system were sulfate anions and their concentration was fixed at 1 M. At higher concentrations of quinones, transfer across the membrane could be insufficient due to a lower proportion of anions. The quinone redox reactions produced and consumed H^+ ions, which were easily transportable due to their small size. Therefore, future experiments may benefit from using a cation-permeable membrane such as Nafion. There is also an abundance of H^+ ions due to the acidic medium used. Hence, cation-permitting membranes might enhance the VE.

Comparison of Energy Efficiency

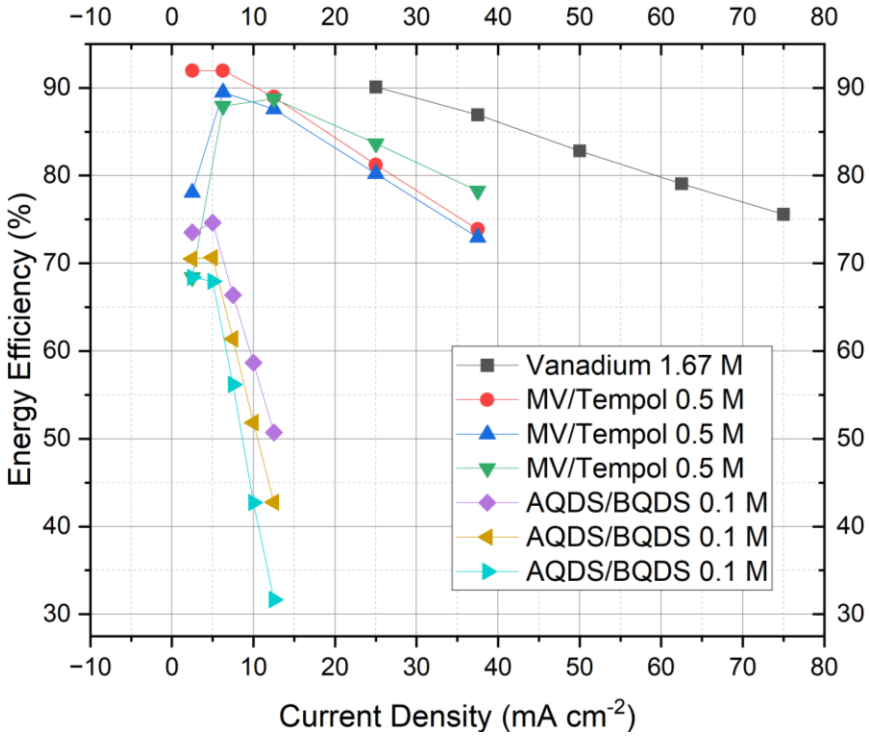

Figure 28: Comparisons of Energy Efficiencies.

From the above plot, it was possible to analyze the efficiency at which the provided energy is obtained back from the battery as useful energy. This depended directly on

the efficiency at which the provided energy was stored in the system (CE) and the efficiency at which it could be used up without loss (VE). We see from **Figure 28** that despite the organic systems having very good CE, the stored energy wasn't fully usable because of several losses as indicated by their low VE. So, the EE of organic systems fell below the EE of Vanadium.

Comparison of Energy and Power Density

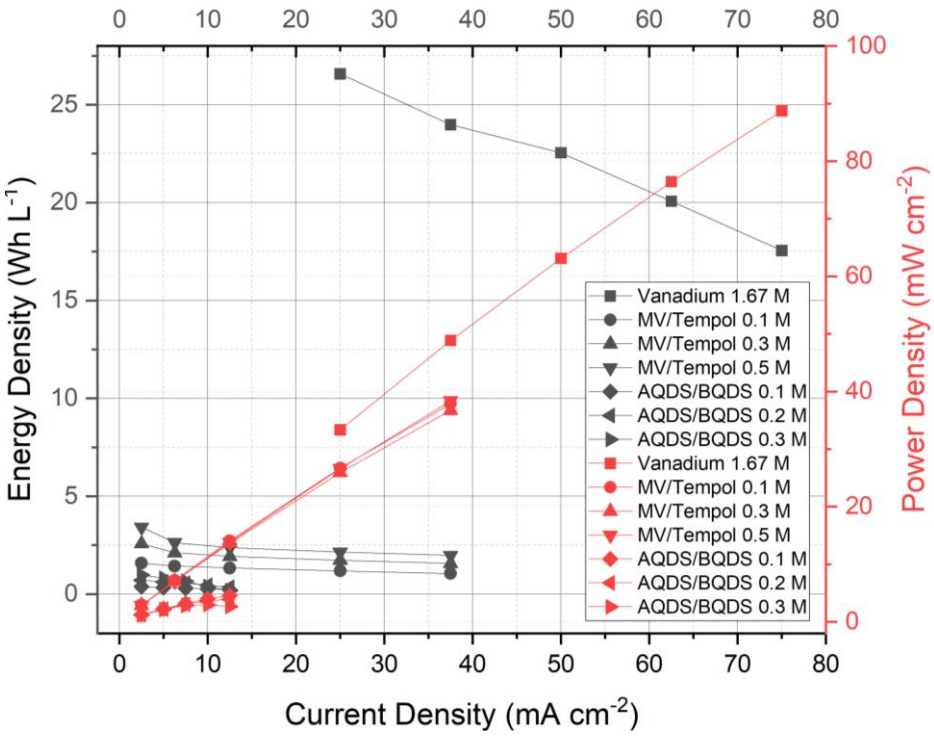

Figure 29: Comparison of Energy Density (**Left-Black**) and Power Density (**Right-Red**).

In terms of energy density, the organic systems really did fall short compared to the Vanadium system. As expected, energy density increased with an increase in electrolyte concentration due to the presence of more energetic materials at higher concentrations, in the same volume. The energy density of quinones was observed to be much lesser than expected. To start with, the E^0_{cell} of Quinones was only 0.74 V compared to 1.25 V for the other two cases. Quinones was also assumed to undergo a 2 electron transfer redox reaction which should have corresponded to a higher energy density than observed. Quinones can undergo the transfer of 2 electrons in a concerted or stepwise manner[21]. When the latter takes place, an intermediate specie

called semiquinone is formed. If this intermediate is stable enough, the system might not react further depending on the conditions provided.

The galvanostatic cycling profiles of quinones also showed only one voltage plateau. This indicated the possibility that the electron transfer occurring is a single electron transfer contrary to the expected 2 electron process. A complete understanding of this required performing Cyclic voltammetry, which in the interest of time could not be completed as part of this study. So, with the available information, it was only possible to speculate the reason for the low energy density of quinones to be due to single electron transfer. To push the system into a 2 electron process, it needed to be subjected to a wider potential range, in which the system isn't currently stable. So, the first step for future studies should be optimization at a wider voltage range.

The power density as shown in **Figure 29** was independent of concentration. As the amount of energy storing active materials increased with concentration, the time taken for all of it to undergo redox reactions also increased negating any final effect in power. The power density of quinones seemed to be very low. However, MV/Tempol showed promising power densities that were comparable to that of Vanadium systems.

TECHNO-ECONOMIC MODELLING

This section presents FLOTE (FLOw battery Techno Economics), a desktop application developed with detailed sophistication encompassing the entire techno-economic model. FLOTE implements all the parameter dependencies from the original model and seamlessly calculates the number of cells and the volume of electrolytes from provided energy and power ratings, while also determining the cost of energy and power, meeting all the functionalities of the original model. FLOTE is additionally equipped with some powerful functionalities which are described later in this section.

This self-contained app was designed to be completely standalone, requiring no third-party applications or internet connectivity to operate. Upon running a Python script, the user is presented with a visually appealing and intuitive user interface, enabling them to swiftly and easily utilize the app's comprehensive functionalities.

Figure 30: FLOTE - Homepage and the Cost Distribution tab. FLOTE has three main functionalities that are divided into three tabs: Cost Distribution, Sensitivity Analysis, and Customize.

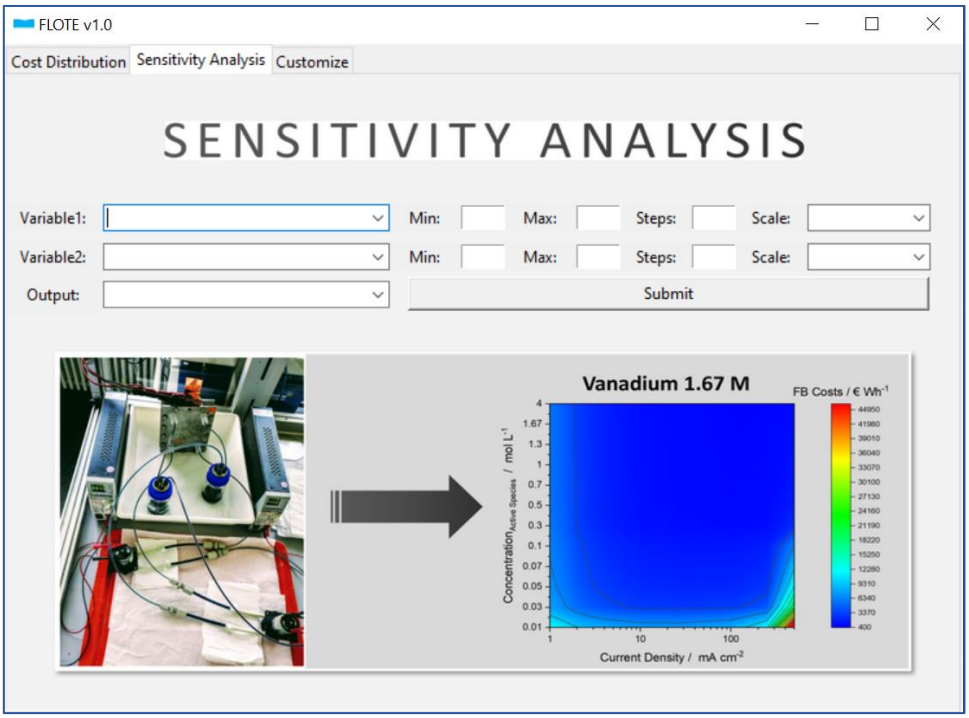

Figure 31: FLOTE - Sensitivity Analysis tab. Users can choose the variable couple they wish to vary and the output format from drop-down menus. They can also set limits between a minimum and maximum value, specify the steps, and even choose to vary linearly or exponentially.

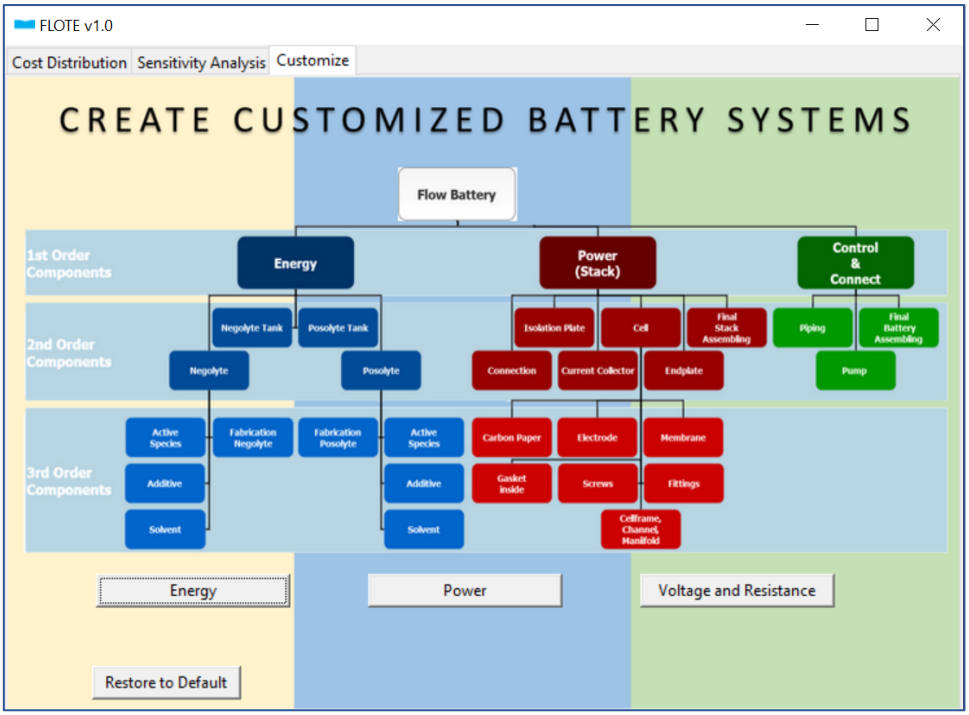

Figure 32: FLOTE - Customize tab. Users can choose to define a new battery system by specifically editing different entries of energy, power, and other buttons. A flow chart is provided to help the user to navigate to the desired component.

Functionalities of FLOTE

Cost Distribution: In this tab, the user is provided with the option to obtain the total battery cost distribution or to visualize the cost components for individual energy and power sections. By default, the application generates cost distribution plots for Vanadium batteries, which were built using standardized cell and electrolyte specifications that were discussed in the theory section. Users may view these default specifications by selecting the 'view default system' button. A typical energy cost distribution is presented in **Figure 33**, with a donut plot representing the first level of the hierarchy and the second level being represented by bar plots on either side in a bar of donuts plot format. **Figure 34** shows a typical power cost distribution, with a sunburst plot used for representation.

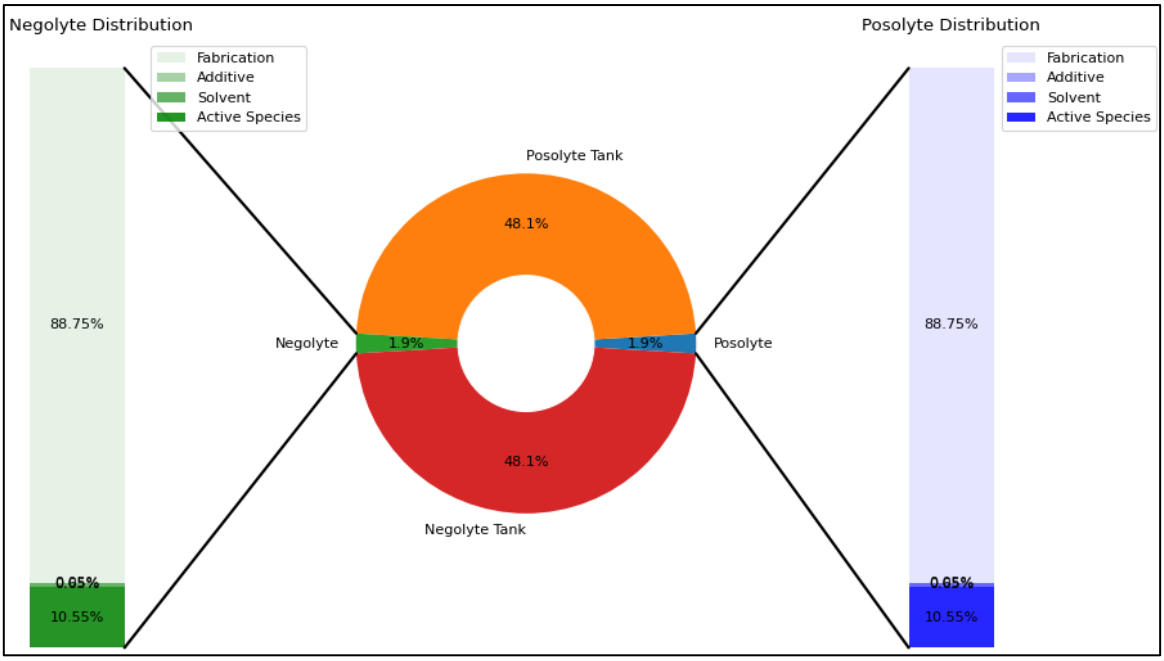

Figure 33: Bar of Donut plot to represent Energy cost distribution. The cost of the tanks seems to predominate the proportion. This is only because of the laboratory scale of the system where DURAN glass bottles with screw tops are generally very expensive. At industrial levels, the cost of tanks can be brought down. Also, the bar plots show a high proportion of fabrication cost which is the cost incurred to have a worker assemble the cell. This can also be reduced at industrial scales through automation and mechanization.

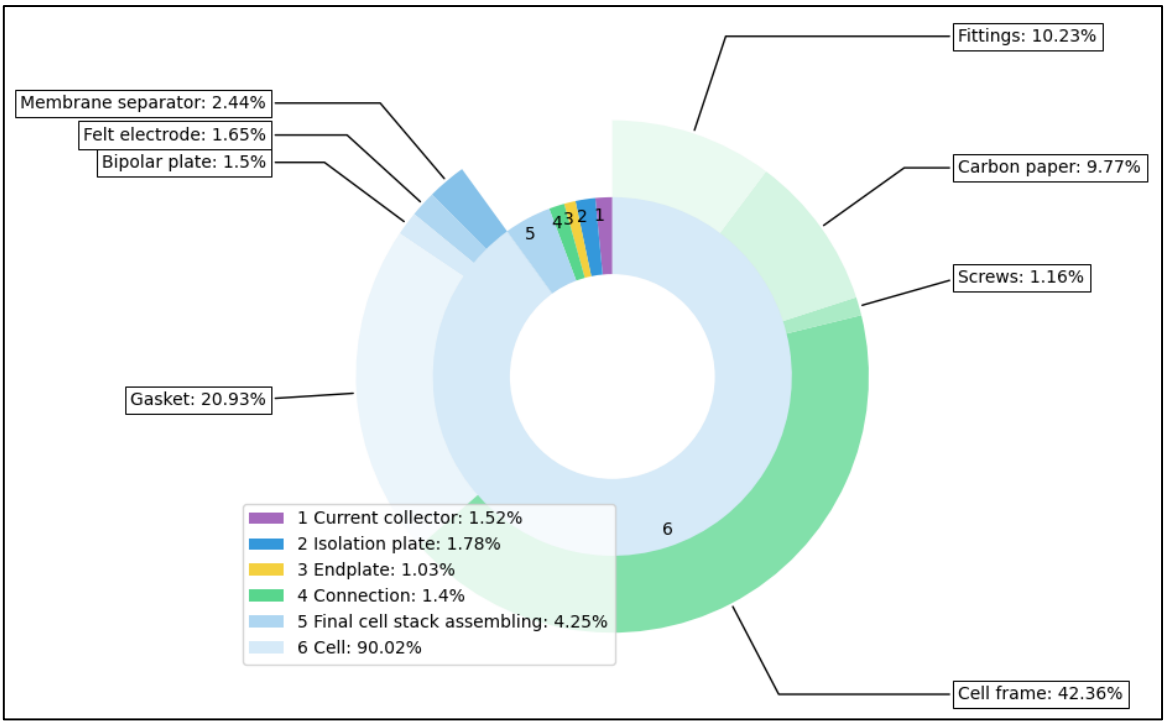

Figure 34: Power cost distribution and its two hierarchies represented using a sunburst plot. Both the gasket and cell frame contribute the most to the total cost of power. The Gasket material is often fragile and experiences tear with prolonged cell use. Hence, from a performance and cost optimization point of view, a replacement material for the currently used gasket material is something worth researching.

Sensitivity Analysis: To perform sensitivity analysis using FLOTE, the user can select the parameter couples they wish to vary from the drop-down list of Variable 1 and Variable 2. Additionally, the output format can be chosen from the output dropdown list. The available variables include cell voltage, current density, and the concentration of active species. The user can select the range, steps, and variation scale with which they want to vary the variables. The output format can be either specific cost per energy content or specific cost per power content. Upon clicking the submit button after entering the relevant details, FLOTE generates and views a contour plot, where one variable is plotted along the x-axis and the other along the y-axis. The output is displayed using colour gradients, and FLOTE also saves the 2-dimensional data as a matrix in a text file.

The FLOTE functionality of automated generation of sensitivity analysis datasheets and plots was observed to reduce the time of task from the order of days to seconds and made the process considerably easier. But the most profound advantage of using FLOTE comes with the possibility to perform sensitivity analysis using all possible variable couples in a matter of seconds. Strong insights into the scientific and engineering sides of battery optimization can be gained with this level of calculations.

Figure 35 shows two sensitivity analysis plots for Vanadium flow batteries generated using FLOTE.

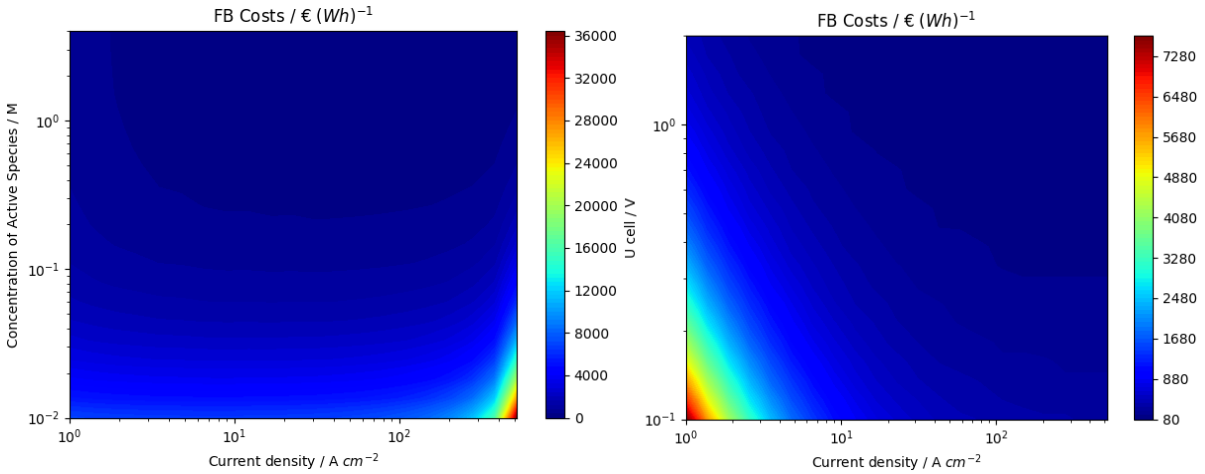

Figure 35: Sensitivity Analysis contour plots generated using FLOTE. Sensitivity Analysis provides information on the areas needing optimization from a cost point of view. From the above two plots, it is evident that the Vanadium system is already fairly optimized with respect to the current density and concentration of active species or cell potential as shown by the majority of blue regions.

Customize: This tab permits users to tailor the techno-economic model's energy, power, and other modules to define their custom battery systems. The parameters that can be edited and entered are always battery parameters that are constants for a given system and are not derived like the active surface area of electrodes, specific price of active materials, etc. Upon launching FLOTE, the editing entries appear pre-populated with the parameter values of a standard Vanadium flow battery. Users are able to select which entries they wish to modify guided by a flowchart. Once a new battery system is defined, the user may then examine the cost distribution or perform sensitivity analysis on the newly customized battery system.

Creating a new system does not destroy the original Vanadium system. The user can always revert all values to the default Vanadium system by clicking on the ‘restore to default’ button.

Figure 36 shows the window where the battery parameters contributing to energy can be edited.

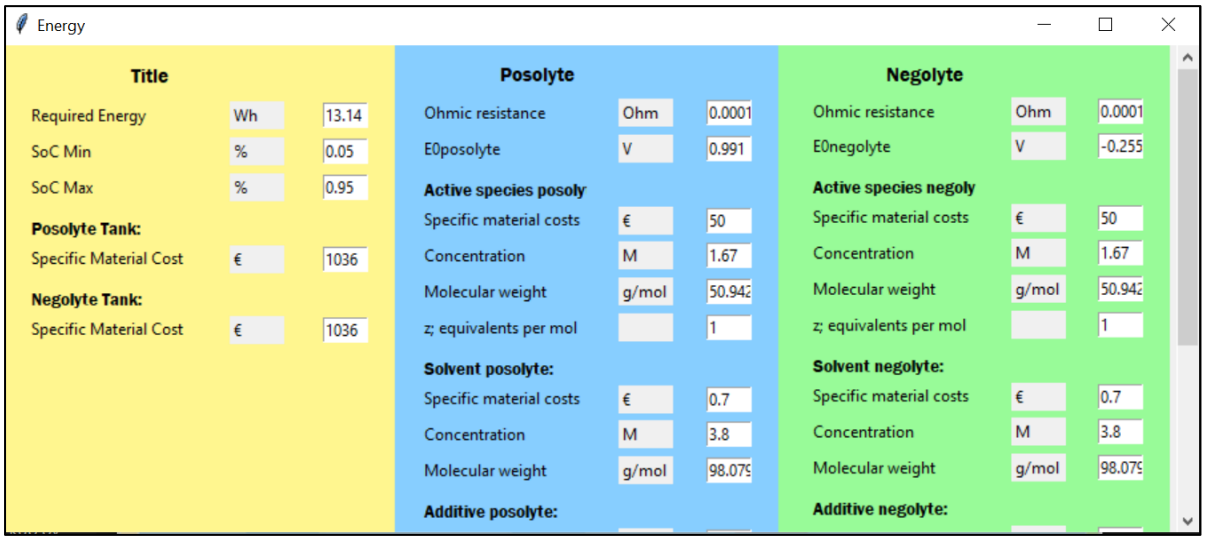

Figure 36: A window where the energy parameters can be edited. The pre-filled values correspond to that of a standardized Vanadium cell.

Cost comparisons of Vanadium and Organic Flow Batteries

FLOTE was used to calculate the cost of energy and power for all three-battery systems given an energy and power rating. The cost of energy depended on the volume of electrolyte needed and the cost of power on the number of cells needed in

the stack. For this, a power rating of 10 W and an energy rating of 100 Wh were chosen for all batteries. The results are summarised in **Table 3**:

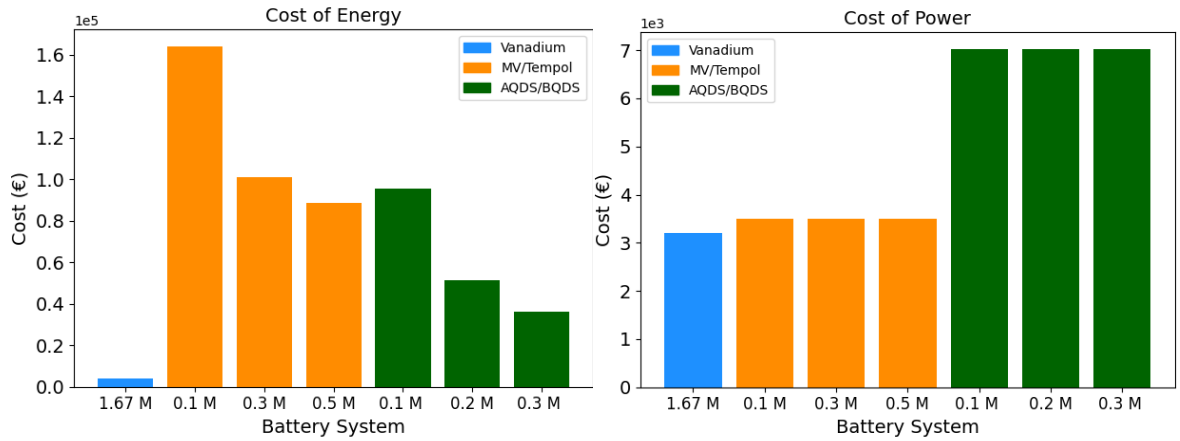

Figure 37: Comparisons of costs.

Battery	Current Density (A cm^{-2})	Cost of Power (€)	Number of cells	Power (W)	Cost of Energy (€)	Volume of electrolyte (L)	Energy (Wh)	Specific Cost of Battery (€ $(Wh)^{-1}$)
V 1.67 M	25	3197.182	8	10	3941.489	3.768718	100	71.38672
MV/T 0.1 M	25	3491.116	9	10	164025.4	90.65816	100	1675.166
MV/T 0.3 M	25	3491.116	9	10	101214.3	30.21939	100	1047.054
MV/T 0.5 M	25	3491.116	9	10	88652.08	18.13163	100	921.432
Q 0.1 M	25	7018.319	21	10	95430.14	85.42992	100	1024.485
Q 0.2 M	25	7018.319	21	10	51174.5	42.71496	100	581.9282
Q 0.3 M	25	7018.319	21	10	36422.63	28.47664	100	434.4094

Table 3: Cost comparisons of Vanadium (V), MV/Tempol (MV/T), and Quinone (Q) systems.

According to **Figure 37** and **Table 3**, the costs of organic batteries were calculated to be greater than Vanadium. But it is crucial to understand that this is so only because the calculated costs were based on organic chemical price for a laboratory amount of 100 g from Sigma Aldrich while the Vanadium electrolyte was obtained at an industrially upscaled price from Fraunhofer ICT. Even such inequitable comparisons show ORFBs to be costlier only by an order than VRFBs. With upscaling of organics, it might be possible to produce cheaper MV/Tempol and Quinone batteries which could potentially be cheaper than Vanadium batteries.

Intriguingly, the cost of energy decreased at higher concentrations of active species. This study considered the specific cost of active material per mass and the mass of active materials requisite to provide a specific energy amount should be independent of concentration. Nevertheless, the cost reduced because the volume of electrolyte required to deliver the said energy (in this case 100 Wh) was lesser at higher concentrations of active materials. This would require only smaller tanks to contain the electrolyte. As evident from the energy cost distribution in **Figure 33**, the cost of tanks contributed significantly to the total cost of the system, and increasing the active material concentration reduced the required size of tanks which, by extension, the cost. Therefore, it can be concluded that a higher concentration of electrolyte is always economically worthwhile. Employing techniques that increase the solubility of organic salts, or choosing the right kind of solvents might help realize this.

In the present-day context, there exist some other crucial factors besides cost and performance that carry significant weight in the assessment of the most appropriate energy option, such as biodegradability, toxicity, and sustainability. A comprehensive evaluation of battery systems can only be achieved through the incorporation of all these parameters.

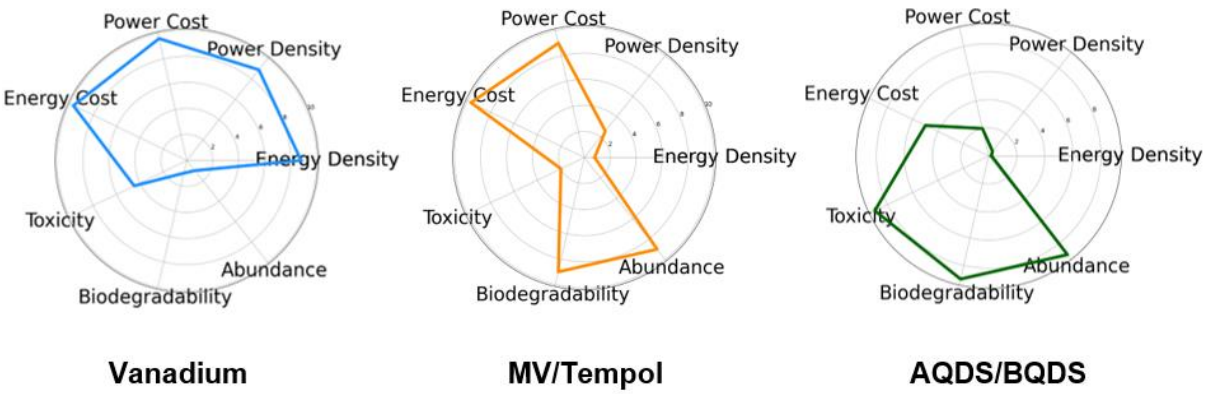

Figure 38: A qualitative comparison of RFBs using 7 different parameters. Each battery was given a score from 0 to 10 for each parameter, with 10 being the most and 0 being the least favorable measure. E.g.- a score of 10 for toxicity or energy cost implies low levels of toxicity and cost.

Overall comparisons like the shown in **Figure 38** have become increasingly valuable in today's context. The spider net plot displays the different domains in which each battery system has its advantages. Vanadium batteries offer excellent energy and power densities at affordable prices but suffer from low biodegradability and abundance. MV/Tempol, an organic system, performs well in terms of biodegradability

and abundance and also exhibits good techno-economic capabilities, but is highly toxic. Quinones exhibit all the green properties but suffer from low energy and power performance, as well as limited techno-economic viability in the current scale of use.

CONCLUSIONS

The present study investigated the performance and chemistry of three distinct flow battery systems, developed computer software for flow battery techno-economic, and utilized it to compare the techno-economic performance of ORFBs with VRFBs.

A previously unreported phenomenon of high initial resistance in MV/Tempol was observed which could be overcome by a low amperage activation cycle. The stable operating voltage, current, and concentration ranges for quinones batteries were identified. ORFBs exhibited excellent CE but lesser VE despite low initial internal resistance indicating issues related to charge transport resistance during cycling. Energy and power densities of organic systems were considerably lower than Vanadium systems owing to several factors except for MV/Tempol's power density which was comparable to Vanadium systems. The primary challenges faced by organic systems were identified as side reactions in the case of MV/Tempol and a rising internal resistance probably due to the use of anion permeable membrane in quinones.

FLOTE, is now available as a software tool, for conducting comprehensive techno-economic analyses of any flow battery system. It allows for the generation of multiple sensitivity analyses and cost distribution plots instantaneously, thereby enabling a detailed investigation into the optimization of ORFBs.

Energy and power cost comparisons of ORFBs with VRFBs performed using FLOTE showed that ORFB costs at the laboratory scale were comparable to the upscaled costs of VRFBs and were only greater by an order. This highlighted the promising future techno-economic potentials of industrially upscaled ORFBs. ORFBs were also qualitatively compared with VRFBs in all overall senses, using seven different parameters from the perspectives of performance, cost, and most importantly sustainability.

The study concludes that it might be possible for ORFBs to attain performance and cost results similar to VRFBs through their optimization. A pH-invariant MV/Tempol

system using buffers could improve its capacity retention. Quinones suffered from high charge transport resistance which could be reduced with the use of ionic salt additives like NaCl, suitable solvents, and cationic permeable membranes. Reducing the current dependant internal resistance might make for a more stable battery opening up a larger operating voltage range. Achieving this might enable one to harness the two-electron redox process of quinones which could double the energy density.

REFERENCES

(1) Renewables 2021 Global Status Report; ISBN 978-3-948393-03-8; REN21: Paris: REN21 Secretariat, **2021**. https://www.ren21.net/wp-content/uploads/2019/05/GSR2021_Full_Report.pdf.

(2) Weber, A. Z.; Mench, M. M.; Meyers, J. P.; Ross, P. N.; Gostick, J. T.; Liu, Q. Redox Flow Batteries: A Review. J. Appl. Electrochem. **2011**, 41 (10), 1137–1164. https://doi.org/10.1007/s10800-011-0348-2.

(3) Gentil, S.; Reynard, D.; Girault, H. H. Aqueous Organic and Redox-Mediated Redox Flow Batteries: A Review. Curr. Opin. Electrochem. **2020**, 21, 7–13. https://doi.org/10.1016/j.coelec.2019.12.006.

(4) Noack, J.; Wietschel, L.; Roznyatovskaya, N.; Pinkwart, K.; Tübke, J. Techno-Economic Modeling, and Analysis of Redox Flow Battery Systems. Energies **2016**, 9 (8), 627. https://doi.org/10.3390/en9080627.

(5) SONAR - Modelling for the search for new active materials for redox flow batteries. https://www.sonar-redox.eu/en/H2020-project-SONAR.html.

(6) Qi, Z.; Koenig, G. M. Review Article: Flow Battery Systems with Solid Electroactive Materials. J. Vac. Sci. Technol. B Nanotechnol. Microelectron. Mater. Process. Meas. Phenom. **2017**, 35 (4), 040801. https://doi.org/10.1116/1.4983210.

(7) GINER, J.; CAHILL, K. Advanced Screening of Electrode Couples; NASA, **1980**. https://core.ac.uk/reader/42865295.

(8) Sum, E.; Skyllas-Kazacos, M. A Study of the V(II)/V(III) Redox Couple for Redox Flow Cell Applications. J. Power Sources **1985**, 15 (2–3), 179–190. https://doi.org/10.1016/0378-7753(85)80071-9.

(9) Winsberg, J.; Hagemann, T.; Janoschka, T.; Hager, M. D.; Schubert, U. S. Redox-Flow-Batterien: Von Metallbasierten Zu Organischen Aktivmaterialien. Angew. Chem. **2017**, 129 (3), 702–729. https://doi.org/10.1002/ange.201604925.

(10) Khataee, A.; Pan, D.; Olsson, J. S.; Jannasch, P.; Lindström, R. W. Asymmetric Cycling of Vanadium Redox Flow Batteries with a Poly(Arylene Piperidinium)-Based Anion Exchange Membrane. J. Power Sources **2021**, 483, 229202. https://doi.org/10.1016/j.jpowsour.2020.229202.

(11) Kwabi, D. G.; Ji, Y.; Aziz, M. J. Electrolyte Lifetime in Aqueous Organic Redox Flow Batteries: A Critical Review. Chem. Rev. **2020**, 120 (14), 6467–6489. https://doi.org/10.1021/acs.chemrev.9b00599.

(12) Liu, T.; Wei, X.; Nie, Z.; Sprenkle, V.; Wang, W. A Total Organic Aqueous Redox Flow Battery Employing a Low Cost and Sustainable Methyl Viologen Anolyte and 4-HO-TEMPO Catholyte. Adv. Energy Mater. **2016**, 6 (3), 1501449. https://doi.org/10.1002/aenm.201501449.

(13) China Electric Power Research Institute; Li, X.; Wang, S.; China Electric Power Research Institute. A Review on Energy Management, Operation Control and Application Methods for Grid Battery Energy Storage Systems. CSEE J. Power Energy Syst. **2019**. https://doi.org/10.17775/CSEEJPES.2019.00160.

(14) Huskinson, B.; Marshak, M. P.; Suh, C.; Er, S.; Gerhardt, M. R.; Galvin, C. J.; Chen, X.; Aspuru-Guzik, A.; Gordon, R. G.; Aziz, M. J. A Metal-Free Organic–Inorganic Aqueous Flow Battery. Nature **2014**, 505 (7482), 195–198. https://doi.org/10.1038/nature12909.

(15) Yang, B.; Hoober-Burkhardt, L.; Wang, F.; Surya Prakash, G. K.; Narayanan, S. R. An Inexpensive Aqueous Flow Battery for Large-Scale Electrical Energy Storage Based on Water-Soluble Organic Redox Couples. J. Electrochem. Soc. **2014**, 161 (9), A1371–A1380. https://doi.org/10.1149/2.1001409jes.

(16) Sihvo, J.; Stroe, D.-I.; Messo, T.; Roinila, T. Fast Approach for Battery Impedance Identification Using Pseudo-Random Sequence Signals. IEEE Trans. Power Electron. **2020**, 35 (3), 2548–2557. https://doi.org/10.1109/TPEL.2019.2924286.

(17) Bischof, K. Technoökonomie Für (Organische) Redox-Flow-Batterien – Untersuchung Einer Standardisierten Laborzelle, Ulm University, Fraunhofer ICT.

(18) Vailshery, L. S. Most Used Programming Languages among Developers Worldwide as of 2022; Statista, **2022**. https://www.statista.com/statistics/793628/worldwide-developer-survey-most-used-languages/#statisticContainer.

(19) Bauer, S.; Namyslo, J. C.; Kaufmann, D. E.; Turek, T. Evaluation of Options and Limits of Aqueous All-Quinone-Based Organic Redox Flow Batteries. J. Electrochem. Soc. **2020**, 167 (11), 110522. https://doi.org/10.1149/1945-7111/aba338.

(20) Orita, A.; Verde, M. G.; Sakai, M.; Meng, Y. S. The Impact of PH on Side Reactions for Aqueous Redox Flow Batteries Based on Nitroxyl Radical Compounds. J. Power Sources **2016**, 321, 126–134. https://doi.org/10.1016/j.jpowsour.2016.04.136.

(21) Tarumi, M.; Matsuzaki, Y.; Suzuki, K. Theoretical Study on the Redox Reaction Mechanism of Quinone Compounds in Industrial Processes. Chem. Eng. Sci. **2019**, 199, 381–387. https://doi.org/10.1016/j.ces.2019.01.006.